Load Bearing Interface Design for a Pan-Tilt Mechanism for Severe Marine Environments

by

Michael John Beautyman, Jr.

Submitted to the Department of Mechanical Engineering
in partial fulfillment of the requirements for the degrees of

Naval Engineer

and

Master of Science in Mechanical Engineering

at the

MASSACHUSETTS INSTITUTE OF TECHNOLOGY

June 2017

Author . Signature redacted .....
Department of Mechanical Engineering
May 12, 2017

Certified by ..... Signature redacted ..
Alexander H. Slocum
Pappalardo Professor of Mechanical Engineering
Thesis Supervisor

Accepted by ..... Signature redacted .
Rohan Abeyaratne
Chairman, Committee on Graduate Students

See Appendix E - Drawings

Load Bearing Interface Design for a Pan-Tilt Mechanism for Severe Marine Environments

by

Michael John Beautyman, Jr.

Submitted to the Department of Mechanical Engineering
on May 12, 2017, in partial fulfillment of the
requirements for the degrees of
Naval Engineer
and
Master of Science in Mechanical Engineering

Abstract

The Naval Research Laboratory (NRL) requested the design of a two-axis gimbal device for the shipboard support of a sensor payload. Previous design efforts presented a low-mass two-axis (pan and tilt) machine. Vibration and shock testing induced failure in the interface between the payload and the tilt shaft, through which the control cabling connected to the sensors, taking the system out of service and creating a hazard for Sailors. This thesis proposes a tapered, hollowed shaft and flange interface connected by an interference fit that is preloaded and retained by a single hollowed bolt for ease of maintenance at sea.

This simplified design is a departure from existing rotary tapered interfaces, such as seen in machine tooling, and focuses on connecting massive payloads to their actuators when subjected to severe loading. This design is uniquely suited to withstand large bending moments and loading as demanded by military standards for shock. A custom rig was designed and constructed to subject reduced-scale designs to military standard environmental testing for shock in the laboratory. These test results were analyzed using moving average filtering to develop confidence intervals to validate the design mathematics. A full-scale prototype was manufactured and subjected to shock testing and analysis. The design exceeded all requirements and is ready for immediate integration into the gimbal. This research also revealed the potential for tapered interfaces to connect massive payloads to their actuators in industry.

Thesis Supervisor: Alexander H. Slocum
Title: Pappalardo Professor of Mechanical Engineering

Acknowledgments

Thank you to my advisor Alex, helped me simplify the hard problems and understood when a long run was the solution. Steven Shepstone gave me hours of his personal time to keep me from reinventing the wheel where possible. Dr. Barbara Hughey provided me sensors, measurement techniques, help analyzing even the noisiest data, and constant positive energy. Hayami Arakawa and Coby Unger of the MIT Hobby Shop taught me everything I needed to know about machining. Professor Eduardo Kausel guided me on impulses and drop testing. Josh Dittrich provided a perfect reduced-scale model and good feedback on the manufacturing process. Andy Gallant of the MIT Central Machine Shop was generous with his time, expedited my job requests, provided valuable feedback to improve the manufacturability of the design, and enthusiasm that reminded me why I work so hard.

The PERG lab is full of generous people eager to help and deserving of thanks, particularly Nevan Hanumara for his resourcefulness, David Taylor and Kevin Simon for showing me where everything is, and Hilary Johnson and Maha Haji for guiding me through MakerWorks. A special thank you to Tom Finley, who spent countless long days and nights discussing design ideas, reviewing plans, providing encouragement, and reminding me to "send it" when I was slowing down. This thesis research ran in parallel to an intensive design course project, which would not have been possible without the incredible efforts of my teammates Randy Jagoe and Jess Olena. Thank you both for taking the weight when I could not.

This thesis is the product of a community effort. MIT EMS gave me encouragement, friendship, and trust. The membership retained faith in my leadership even as I reduced my involvement to pursue my thesis, and I am so proud of everything you all achieved this year. The future is very bright. Thank you Maryanne Kirkbride for the love, the tough love when I needed it, and always letting me know you have my back.

Amanda Yanchury tolerated what should have been an insufferable schedule, bringing me dinners in the office and encouragement every day. Thank you for understanding when my focus was elsewhere and for pardoning my frequent absence in the spring. Alexandra Beautyman and Victor Mutai were incredible, providing me with schedule management, proof-reading, code review, research assistance, enthusiasm and support, and even a week of meal prep so I could stay focused near the end.

I am lucky to be supported by such an amazing collection of people.

THIS PAGE INTENTIONALLY LEFT BLANK

Contents

THIS PAGE INTENTIONALLY LEFT BLANK

List of Figures

List of Tables

THIS PAGE INTENTIONALLY LEFT BLANK

Chapter 1

Introduction

This design thesis was inspired by a system design problem put forth by the sponsor, the Naval Research Laboratory (NRL). In 2014, the NRL asked the Precision Engineering Research Laboratory (PERG) to "design, build, and test a two-axis pan tilt mechanism for shipboard use to support an NRL project" on which a "key feature is that the elevation mechanism's axis of rotation will be based on a large diameter bearing such that the payload be placed at and project through the elevation mechanism." [Slocum, 2014] The resulting directional device machine is meant to focus in a specific direction along the azimuth and elevation as commanded by precision motor controllers. The machine must be design for exposure to green water (seawater which washes over the deck of a ship), wind loading, vibrations, and shock. The NRL is developing the payload, for which specifications are classified. All discussions of the payload in this thesis refer only to geometry and mass without detail of capability or purpose.

From 2015-2016, Nathan Mills brought the project through prototyping and initial testing. This testing revealed component failures that required new designs in order to meet NRL specifications. Critical among these design failures was the interface

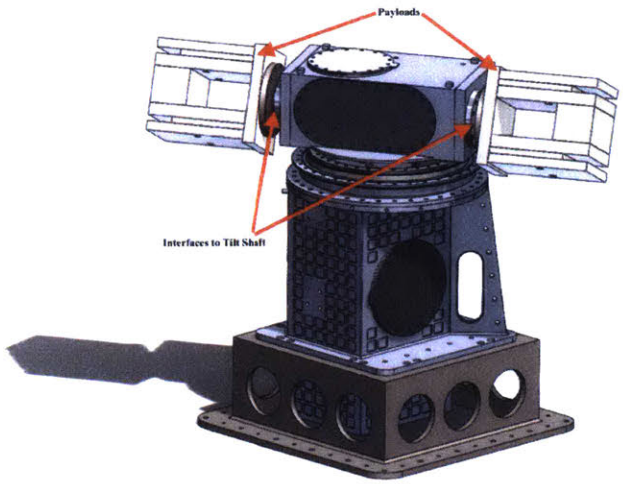

Figure 1-1: Gimbal model [Mills, 2016]

joining the payloads to the horizontal shaft actuator (tilt shaft) that controls the rotation of the payloads to their zenith.

This thesis details the research, design, prototyping, and testing of an improved interface between the payloads and the tilt shaft, and its possible applicability beyond the mechanism specified by the NRL. This thesis also discusses the design of rigs to test the interface to the specified military standards within the laboratory. This thesis is unclassified.

The design process began with a review of literature on mechanical interfaces in robust systems, found in chapter 2. This ranged from patents for aviation components to discussions of high-speed tooling machinery. This research provided a baseline for the development of innovative interface designs and provided exposure to the existing methods for connecting payloads to shafts on rotating systems. It also ensured that no design effort would be duplicative or infringe on existing design patents.

From this effort came several candidate design solutions, detailed in section 3.1. These were analyzed for compliance to the NRL specifications as well as for simplicity, part count, maintainability, and weight. Section 3.2 discusses the design process

and the development of mathematical models to facilitate rapid analysis of different designs, and section 3.5 reviews the manufacturing process for the reduced-scale model.

Sections 3.4 and 3.6 detail the design and manufacture of shock tests intended for a reduced-scale prototype in the laboratory and for a full-scale model. Due to the large mass of the actual payloads, different testing rigs were required for the reduced-scale and full-scale interfaces. This chapter also discusses the characterization of these rigs in order to control each experiment.

Chapter 4 presents the results and analysis of those shock tests, with observations about features of the test rigs and interfaces that influenced the data. This chapter also discusses the applicability and integration of this design to the NRL gimbal, and the potential applicability of this interface design for other systems connecting massive payloads to actuators. It concludes with a discussion of future work.

1.1 Requirements

1.1.1 Sponsor Requirements

Table 1.1 is a summary of the sponsor requirements pertinent to this research. Of particular importance to this thesis are the angular accelerations, payload size and mass, wind loading, wave loading, vibration, and shock requirements. The geometry of the payload was approximated from a mock-up model provided by the sponsor. This allowed for fairly accurate assumptions in calculating moments of inertia, distances, and other geometric quantities. The angular accelerations, wind and wave loading values, and the vibration and shock standards were used to calculate the maximum forces and moments on the machine.

Table 1.1: NRL requirements

Criteria	Threshold	Objective
Max angular speed $[deg/s]$	50	100
Max angular speed $[deg/s^2]$	50	100
Payload mass total $[lbm]$	130	170
Payload dimensions each $[in]$	9 x 7.5 x 6	
Green water loading	6 $[psi]$ on full frontal area	
Wind loading without damage	115 $[kts]$ sustained, 120 $[kts]$ gust	
Vibration Resistance to MIL-STD-167-1A	4-15Hz: table amplitude 0.030in 16-25Hz: table amplitude 0.020in 26-33Hz: table amplitude 0.010in	
Shock Resistance	MIL-S-901D	
Cable Bundle	20 $[mm]$ diameter	

1.1.2 Derived Requirements

My experience at sea as a Naval Officer informed several requirements, as did the lean principle of poka-yoke, or the reduction of chances for operator error. Simplicity was critical for assembly and disassembly on a moving vessel in a variety of conditions. Simplicity also informs maintainability - the ease with which Sailors could work on the interface while at sea. Ships spend the majority of their time far from their supply depots, and have limited cargo space for spare and replacement parts. For this reason, a reduced part count - another component of simplicity - was essential. All design efforts favored manufacturability where possible in order to reduce cost.

The interface design was developed from a mathematical model that predicted the ability of the interface to hold the payloads through all requirements. In order to validate this mathematical model, I designed and constructed a shock test in the laboratory. The full-scale model also required testing. Both of these tests had to impart large shock loads, meaning they were constructed to withstand those loads while providing a stable platform for measurement. Additionally, the accelerometer sensors used were bandwidth limited, meaning that they had a specific frequency

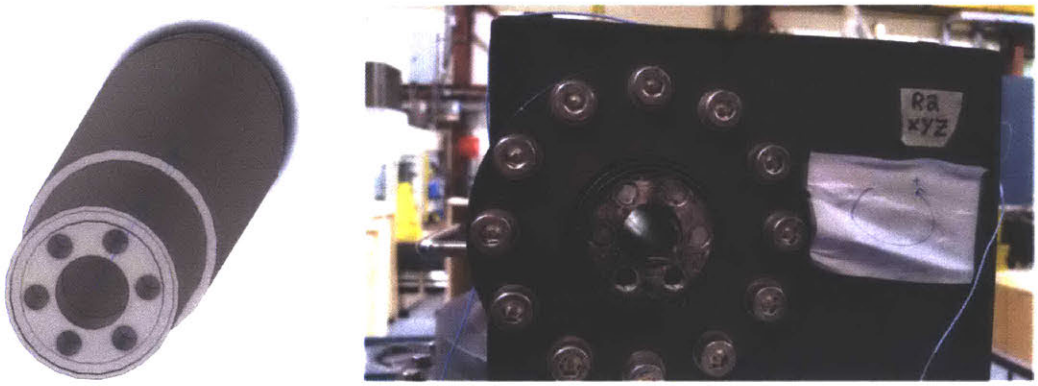

Figure 1-2: The model and shock test results for the old interface

range over which they could operate and collect data. This meant designing the tests to control for the time interval of the shock test impulse to ensure the accelerometers would gather multiple data points across the peak acceleration. Chapter 3 discusses these test requirements in detail.

1.2 Characterizing the Problem

In the first iteration of the gimbal [Mills, 2016], the payloads connected to the tilt shaft via a circular 6-bolt pattern. These bolts were driven into the flat of the circular end face of the cylindrical shaft. During vibration and shock testing, this interface failed when the bolts sheared, causing the payloads to partially sever from the tilt shaft.

The existing geometry of the gimbal tilt housing constrained the general solutions for redesigning the tilt shaft. For example, the bearings on which the tilt shaft sit in the tilt housing defined the maximum shaft diameter and thus the maximum diameter of the tapered interface. These constraints are enumerated in section 3.7. The challenge was to redesign the shaft and interfacing components to withstand the required forces and moments while maintaining simplicity, manufacturability,

maintainability, and a low part count. In addition I avoided adding mass to the system and to reduced the number of parts required.

1.3 Executive Summary

The Naval Research Laboratory (NRL) requested the design of a two-axis gimbal device for the shipboard support of a sensor payload. Previous design efforts (Mills, 2016) presented a low-mass two-axis (pan and tilt) machine. Vibration and shock testing induced failure in the interface between the payload and the tilt shaft, through which the control cabling connected to the sensors, taking the system out of service and creating a hazard for Sailors. This thesis proposes a tapered, hollowed shaft and flange interface connected by an interference fit that is preloaded and retained by a single hollowed bolt for ease of maintenance at sea. This simplified design is a departure from existing rotary tapered interfaces, such as seen in machine tooling, and focuses on connecting massive payloads to their actuators when subjected to severe loading. This design is uniquely suited to withstand large bending moments and loading as demanded by military standards for shock.

The first iteration of the interface was a circular bolted pattern as pictured, which failed in shear during vibration and shock testing of the full gimbal. The gimbal was required to withstand green water loading, wind loading, select MIL-STD-167-1A vibrations, and MIL-S-901D shock. This interface, which moves the payloads, also needed to provide enough torque to do so without slipping circumferentially or axially. The shock requirement is the most demanding of these requirements, so I focused on that noting that the other requirements would be met as a result. I also derived several requirements from my own experience at sea and from the lean principle of poka-yoke, or the reduction of chances for operator error. Manufacturability, simplicity and

repeatability in assembly and disassembly, and a low part count were critical.

To meet these requirements I considered and rejected several potential solutions: a larger shaft and bolt pattern (bearing restricted), a helicopter-style rotary joint (too complex), a wind turbine joint (too many parts), and others. The optimal solution was a tapered interference fit, which facilitated repeated removal and replacement of the connecting flange while still providing a substantial retaining force and resisting shock-induced bending moments. Utilizing a commercially available flat head screw to provide the pre-load and retention reduced cost and part count while keeping the design familiar to the maintaining Sailor.

The design of the interface required examining existing tapers, such as those used for high-speed tooling, in automotive work, and in fastening ship propellers to their shafts. From these areas I obtained standards for tapers that could guide my design, though this use was unique in featuring multi-directional forces and moments and in seeking a reduced footprint. Solving by hand at first, I developed an equation for the ability of the taper to resist a bending moment due to shock. In the equation below, M represents that resisting moment for 90 degrees of the taper revolved around the x-axis, for a total resistance of four times that value.

The design required readily available shock testing, as the formal testing previously conducted was costly, time-intensive, and not local. I researched and rejected explosive testing (dangerous, difficult to setup, difficult to repeat) and simple drop testing (generally limited by bandwidth of available accelerometers) before settling on impact testing. Inspired by Charpy testing machines, I developed a mathematical spreadsheet that calculated the acceleration experienced by a mass on a fully characterized physical pendulum released from a given angle. I specified, designed, machined, and assembled a pendulum rig and components that contacted a large compression spring at the bottom of its arc, creating a known acceleration as a function of the spring constant

and geometric and mass properties.

The pendulum rig and the predicted accelerations were validated using a test mass bolted to the pendulum arm, on which two accelerometers were attached. The pendulum rig was bolted in place and stiffened to ensure the accelerometers did not get poor data from movement of the system. Even so, the data collected was noisy from vibrations in the pendulum arm and the sensor mount. After adding a damper to the pendulum arm, I passed all results through a smoothing filter to account for the outlying data points. This filter used a moving mean. To determine the window over which the mean would be calculated, I plotted the sum of absolute differences between the smoothed and noisy data for different window sizes and identified the knee in the curve, noting that the maximum acceptable window was equivalent to the number of data points collected during the total impulse time. These results were then compared to the predicted values to develop confidence intervals for the test data.

After thus validating the pendulum, I had a reduced scale taper shaft and flange manufactured for testing. The pre-load was derived from the Propeller Installation Calculations for US Navy Ships [Shepstone, 2005], while the rest of the design incorporated other research and deviations from the standards surrounding tapers. The pre-load was designed to "fail" when subjected to a 20 g-force acceleration, meaning that it would come loose from the shaft. The flanges were pressed onto the shaft, and the bolts partly backed out to permit movement while securing the flanges from leaving the test rig entirely. As predicted, the model came loose at 20 g-force.

After validating the design code mathematics, I developed the full-scale model. This model was designed to meet the existing tilt shaft housing parameters, and thus was partially geometrically defined, such as in diameter where the bearings sit. Taking advantage of the additional resistance afforded by the hollowed bolt, and the ability

to increase the pre-load if desired, I reduced the engagement length of the interface to decrease the footprint of the gimbal. The full-scale tilt shaft was manufactured partially solid in the center to permit shock testing without collapse or other damage.

The full scale model was too massive for testing on the pendulum rig and required a drop test. For this, I developed a simply-supported beam that acted as a spring in series with the tilt shaft "beam," from which I could predict the acceleration when dropped from a given height. The intent of this test was to prove 60 g-force capability and then continue upwards until unable due to system failure or inability to test further. The tilt shaft and payload system was rigged to a shop crane using a tumble hitch, a stable quick-release knot used to support heavy loads without jamming. Neither the interface nor the simply supported beam failed during testing, and I was forced to conclude when I could no longer lift the shaft and payloads higher.

The data collected from the full-scale drop test was plotted and found to be significantly less noisy than the pendulum rig data. The impulse time contained approximately 26 data points, and the peaks of the 500 g-force accelerometer results comprised upwards of 17 points, indicating reliable maximum value data. For comparison, I still plotted a moving average of the data using the window size dictated by the sum of absolute differences plot.

This tapered interface successfully met the requirements for the gimbal and may be utilized in the prototype machine. It reduces the part count and the time required for maintenance and repair. It could be further reduced in size, but that would require an increase in pre-load and thus application torque. This design proves that tapers are a feasible method to connect massive loads to their actuators, and can use different geometry than established in automotive and marine industries. There is potential to use this technology with large actuators in industry. Future work on this project could include making a graphic user interface for the code such that a designer could

input some parameters and have a taper design iterated from the code.

Chapter 2

Literature Review

2.1 Introduction

The ubiquity of shafting interfaces in machine tooling and the marine industry has generated a substantial amount of analysis and research into their design and development. Although the literature covers a wide variety of analysis, this review will focus on three major themes that emerged throughout the research. These themes are: types of interfaces, interface mathematics, design, and dimensioning, and interface manufacturing. In addition, this literature review examines shock testing mechanical systems as required by this thesis. From this review, I developed potential interface designs and parameters to address the gimbal interface failure. While there were many resources relating interface design to torque, very little was available that explicitly discussed bending moment resistance. In fact, bending moments were listed as a tertiary function of tapered interfaces [Bossmanns and Tu, 2002].

2.2 Types of Interfaces

There are a variety of shafting interfaces used, mostly either bolted or tapered. Tapered interfaces range from the German HSK to the American CAT [Agapiou, 2005]. As the popularity of tapered tooling interfaces increased, designs such as $^{7}/_{24}$ [Bossmanns and Tu, 2002] and KM [Lewis, 1999] were developed. Yet another article discussed the Japanese-designed BT shank and the attempts at standardizing taper designs geographically, as the author predicted the decline of steep-taper systems in the face of cheaper, quality standard tapers [Kocherovsky, 2000]. All of these tapered interfaces are designed for transmitting torque in rotating systems. While some of these systems build in protection through intentional slip, that is not a desired feature for the gimbal tilt shaft interface. These articles did not explore the bending moment resistance of these interface designs.

2.3 Interface Mathematics, Design, and Dimensioning

2.3.1 Mathematics

In addition to presenting the existing interfaces, the literature explored the mathematical models used to create resilient designs for specific purposes. While presenting a potential wind turbine joint design, one paper offered a way to assess the effects of the interference fit, such as the stress and displacement on the hub connecting the load to the cylindrical shaft [Kang et al., 2015]. A structural member can experience axial, torsion, and bending stresses and strains simultaneously. This combined loading can be determined using superposition [Vable, 2002]. The US Navy has sought solutions for securing propellers to tapered shafts. This can be solved using the required thrust and the geometry of the shaft and propeller hub. This provides the interface pressure

and the required push-on force [Shepstone, 2005]. For the purpose of the gimbal tilt shaft interface, this was invaluable information for designing the axial loading screw.

2.3.2 Design

Equally important to the design process as the equations surrounding the design were the lessons on critical features of shafting interfaces. Tapered interfaces are favorable to cylindrical because they are able to be re-tensioned, are detachable, do not significantly weaken the shaft, and are great for centering. Tapers ratios smaller than 1:10 in particular are detachable only with difficulty [Bosch, 2004], rendering them appropriate for a system that will be occasionally disassembled for maintenance. In addition to being optimal for joint centering, tapered interfaces can be most simply and effectively preloaded using a thread, such as the single large screw ultimately used in this design [Creitaru and Grigore, 2011]. Despite these advantages, the stiffest shaft tapers require end contact with the flange, for which the precision requirement is critical [Bossmanns and Tu, 2002].

2.3.3 Dimensioning and Components

While the marine industry has established a standard for long engagement lengths [DNV, 2015,LR, 1982], research shows that longer shaft lengths lead to more vibration [Bashir Asdaque and Behera, 2014]. Combined with the requirement to maintain a small footprint for the gimbal, this suggested that I explore decreasing the size of the taper engagement length. In machining, the tooling structure - the tapered connection - is the weakest link, underscoring the importance of designing a stiff joint [Agapiou, 2005]. Again the axial load from a threaded fastener rose to the top of possible ways to address this design need. Good taper designs are relatively minimal, generally

including three major couplings [Bossmanns and Tu, 2002].

2.4 Interface Manufacturing

It was noted that "improving the stress distribution of the hub is an effective approach to strengthen" a connection [Ling Xiong et al., 2013], suggesting that the design be manufactured to a precision finish and fit. Furthermore, "if precise tolerances are not achieved on the taper and face, both on the male and female taper forms, there can be a negative impact on the performance of the connection." [Hanna et al., 2002]. While press-fit connections can halve the endurance limit of the shaft material, a rolled interface increases endurance [Peterson and Wahl,]. This dictated the manufacturing process to ensure and resilient and robust design.

2.5 Shock Testing

Shock tests are rapid events requiring extensive planning prior to execution. Some are more intensive than others, such as the multiple contact drop test designed to mimic the stresses of dropping small objects like mobile phones [Goyal and Buratynski, 2000]. Even the most simple drop test must be carefully setup. Accelerometers are best mounted with screws and must be chosen with due consideration to the bandwidth limitations of the sensor. Even dropping a 10 $gram$ sensor from 1 m high can result in 30,000 g-forces [Endevco, 2016]. Explosive tests, while realistic, are dangerous, complex to setup, and risk limiting the test sample size to one [Schauer, 1962].

2.6 Conclusion

The literature review revealed best practices for the design of a torque-transmitting tapered interface, and established a tapered interface as the best option for the gimbal tilt shaft interface to the payloads. There was little information available on bending moments for these tapers, which were focused largely on small interfaces for tooling and not on connecting massive payloads to bi-directional actuators. Providing more information on bending moments for massive payload interfaces became a focal point for this thesis.

THIS PAGE INTENTIONALLY LEFT BLANK

Chapter 3

Methods

As noted in Table 1.1, the tilt shaft and payload interface components must transmit torque for elevation positioning, provide axial retention against centripetal forces during azimuth positioning, vibration, or shock loading parallel to the tilt shaft, and resist the bending moment from loading the payloads orthogonally to the tilt shaft by water, wind, vibration, or shock. After observing the original interface fail during testing, Mills noted in his thesis:

> The most destructive forces may be externally imposed due to wave impact or inertial due to shock. Both are expected to be exacerbated as payloads grow in size and weight. The machine . . . began to fail at the relatively benign shock level of 20g. [Mills, 2016]

Of those external forces, shock loading per MIL-S-901D was calculated to be the largest by an order of magnitude. Therefore the bending moment due to shock loading became the primary design concern, as resisting that moment would ensure the interface exceeded the other requirements. As noted in Chapter 2, most shaft to payload interface literature has been dedicated to torque, as in high-speed machining

and automotive design, suggesting that this design effort would be relatively unique.

In addition, this design would only be successful if simple to assemble and maintain on a ship at sea. Keeping the design intuitive was critical.

3.1 Analysis of Alternatives: Interface

The first step was to identify different means for connecting payloads to shafts. The literature review discussed in Chapter 2 identified or inspired a field of torque-transferring designs found in wind turbine construction, railroad cars, helicopter rotary wing attachments, and high-speed tooling for machinery. These ranged from cylindrical interference fits, to bolted features, to multi-part taper systems to establish the connecting friction forces.

Larger Shaft and Bolt Pattern The diameter of the shaft was defined by the bearings on which it rides in the tilt housing, holding it to a maximum 50 mm. A bolted feature mimicked that of the original design which failed shock testing, and was eliminated for predicted failure in shear stress.

Welded Flanges While this solution would offer a very strong connection between the payload flanges and the shaft, it would require a complete redesign of the much more complex tilt housing in order to split the housing and install the shaft. Installation from one end would not longer be possible.

Threaded Tilt Shaft A threaded shaft would allow the payload interface to be screwed on and off. However, such a design could easily be misaligned given the difficult of controlling the end position of a threaded fastener. This design would also induce a high stress concentration at the root of the internal thread on the payload

flange. This would require a removable alignment pin, which - along with the threads themselves - would present an entry point for salt water.

Cylindrical Interference Fit These are attached by either a press fit, requiring an arbor press or similar machinery, or a shrink fit, requiring an intensive heating operation. As this pan-tilt system is meant to be maintained – including possible assembly and disassembly – by Sailors on a ship at sea, such a design was either not possible or not practical. The repeatability of a cylindrical press fit was also a concern, as misalignment is easy and can cause galling on the surfaces of the mating components.

It became clear that a tapered interface would better meet the functional requirements. However, existing designs were overly complex and high part-count.

Helicopter Rotary Joint The literature review identified a patent for a coupling flange system for a hollow shaft connecting a helicopter main rotor and tail rotor. This design used five components that connected a cylinder to a flange via an expanding tapered element internal to the shaft cylinder. However, this requires numerous parts that would be complex to manufacture, a tedious assembly, and provided no means of repeatably aligning the two interfaces of the tilt shaft. Additionally the massive nut used to tighten the system would induce high stress concentrations, and the nut could not be backed off while maintaining pressure.

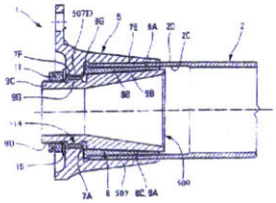

Figure 3-1: Patent drawing for a tapered rotary joint [Mermoz, 2007]

Wind Turbine Joint An article on transmitting torque for a wind turbine proposed using a two-piece tapered collar on a cylindrical shaft, tightened by a bolted flange.

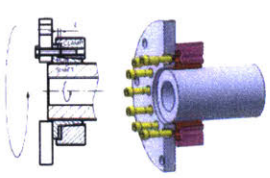

Figure 3-2: Diagram and solid model of wind turbine joint [Kang et al., 2015]

It featured a tapered ring, a split tapered ring, and a flange that attached externally to the shaft cylinder. However, it was secured by a twelve bolt circular pattern, making it a laborious assembly and disassembly process even before connecting the payloads. It offered no features for repeatable alignment port and starboard.

High-Speed Tooling This space of machine design has long relied on tapers to securely and precisely hold tool heads, using technologies such as HSK, BT, CAT, and KM [Lewis, 1999]. However, these tools are often "pulled" into the taper from the opposite side, such as when a collet is installed in a milling machine. The symmetry of the tilt shaft design required that each interface be assembled independently of the other.

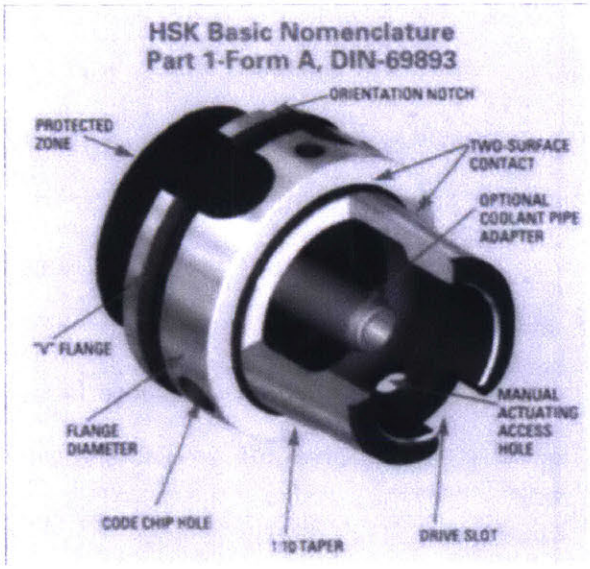

Figure 3-3: HSK Basic Nomenclature [Lewis, 1999]

Marine Joints Like high-speed tooling, propeller interfaces to shafts are designed to transmit torque, albeit at lower speeds and much larger values. The marine

industry has long been using tapered interfaces, for which standards have been provided by several international classification societies such as DNV. These are used for rudder connections, propeller connections, and other interfaces in the ship control systems. These standards often rigidly define the geometry of the taper, and are designed for complex assembly and disassembly using numerous components.

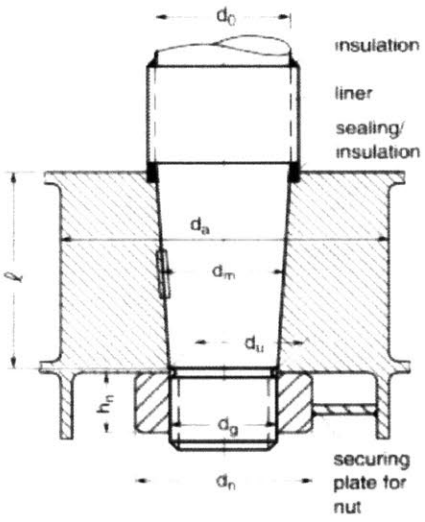

Figure 3-4: Cone Coupling with Key [DNV, 2015]

3.1.1 Selection of Optimal Solution

The interface I was designing needed to be easily manipulated by maintainers ashore and at sea, meaning that alignment, assembly, and removal must be repeatable with basic hand-portable tools and a relatively low complexity/low part-count for when working in austere environments. A keyed taper allowed for a press fit that could be aligned by hand and pushed on. The small key way would ensure alignment between the two payloads. The press fit ensured that the interface would be capable of resisting the bending moment due to shock, of transmitting torque, and of resisting penetration

during green water events. The taper made alignment for installation easy, sticking to poka-yoke principle and reducing the opportunity for the maintainer to induce galling of the material.

The next step was to design a simple tapered interface that could withstand the bending moment due to shock. The first iteration of this idea is seen in figure 3-5. Drawing on the best elements of the helicopter, wind turbine, and propeller designs, I developed an interface wherein the shaft and flange themselves are tapered. The axial force comes from a single large hollow screw that is threaded into the hollow tilt shaft. This permits the control cabling to connect to the payloads, allows a sailor to press on the flange with hand tools, and provides a pre-load to assist the interference fit through vibration and shock.

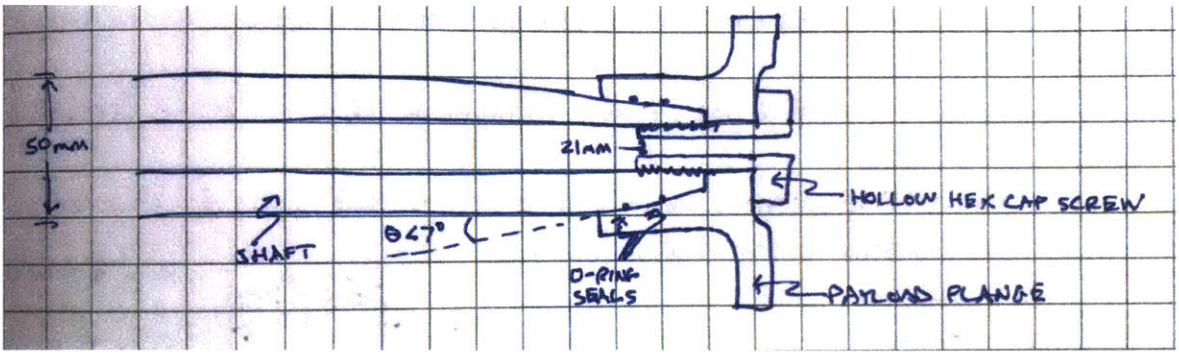

Figure 3-5: Initial design sketch

3.2 Development of the Interface Mathematical Model

3.2.1 Hand Calculations

The holding strength of a tapered interface is dependent upon the pressure exerted between the mating surfaces P, the coefficient of friction μ, the engagement length between the mating surfaces L, the maximum radius of the engaged shaft taper r_{max},

and the taper angle α as defined in Figure 3-6.

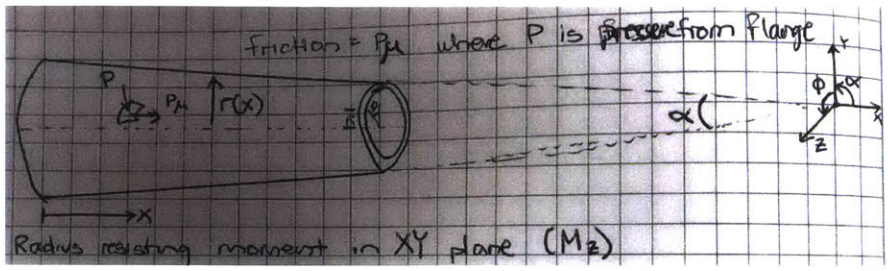

Figure 3-6: Diagram of shaft interface for hand calculations

Integrating over the engaged surface of the shaft taper revealed the governing equation for resisting the bending moment, seen in equation 3.1. The full derivation is included in appendix A.

$$M_{resist} = 4\frac{P\mu}{3}L\sec\frac{\alpha}{2}(L^2\tan^2\frac{\alpha}{2} - 3Lr_{max}\tan\frac{\alpha}{2} + 3r_{max}^2) \tag{3.1}$$

In order to determine the pressure in equation 3.1 I turned to the process used for propeller installation on US Navy ships. This process uses the larger of the required thrusts forward and astern and the dimensions of the taper in a quadratic equation to determine the interface pressure to prevent slip [Shepstone, 2005]. For this design, I determined that the maximum axial shock load - 60 g-force acting on the payload pass - was the required thrust. From this interface pressure and the contact area of the shaft and flange the push-on force was calculated. The next step was to consolidate these mathematical processes.

3.2.2 MATLAB Script

To capture all of the variables contributing to both the Shepstone math and the bending moment equation to facilitate iterating the design through different parameters and scales, I consolidated these calculations in a MATLAB script found

in appendix B. This code also assessed the material ability of all components - shaft, flange, and hollow screw - to ensure no component would fail during operation. This script drew heavily on threaded fastener equations from *Shigley's Mechanical Engineering Design 9th Edition* and Fastenal Engineering & Design Support's *Screw Thread Design.*

In order to validate the mathematics used to design the tapered interface to withstand 60 g-force, I needed to create a shock test that could be conducted locally and without the expense of commercial testing. The script concluded that the full-scale interface design would be able to withstand the shock requirements, as seen in appendix B. In order to validate this model, I iterated to a small version of the shaft and flange with a decreased push-on force and interface pressure. This reduced-scale model was designed to fail at far below the shock requirements. If the prototype performed as predicted, the same mathematics could be used for the larger model.

3.3 Analysis of Alternatives: Shock Testing

Researching shock testing led me to explosive testing, drop testing, and various forms of impact testing.

Explosive Testing Explosive testing is used for subjecting materials and systems to extreme environmental loading, with high heat, forces, and impulses. In particular, U.S. Navy ships are subject to shock testing after construction [Schauer, 1962]. Explosive testing presented concerns around access, safety, cost, complexity, and repeatability. Explosive testing facilities were not readily available and would add cost to the project. I considered conducting testing myself, but the risk and complexity

was prohibitive. Finally, explosive testing would risk the repeatability of the test if any components were to be damaged, jeopardizing the schedule and the tests.

Drop Testing Drop testing offered a more viable solution than explosive testing, using gravity as the means to accelerate the shaft and payload before bringing them to a sudden stop. Numerous methods have been explored in the mobile phone space [Goyal and Buratynski, 2000], but the masses and forces involved in testing this interface are much greater.

I first calculated the parameters of a test wherein I dropped the subsystem (connected shaft and payloads) onto a very stiff surface of known physical characteristics, in this case a steel plate. Using the natural frequency to calculate the impulse forces, time, acceleration, and deflection [Endevco, 2016], I soon recognized that the impulses seen in materials as stiff as the steel of the interface were too rapid. A successful test would require dropping the subsystem from impossibly low heights [Kausel, 2016]. Even if set up, the bandwidth of the available accelerometers would not capture the peak or not collect enough data points during the impulse to present valid data.

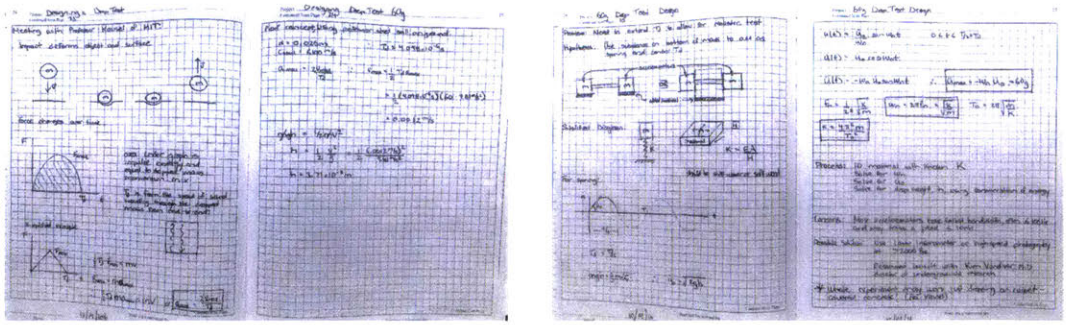

Figure 3-7: Notes on accelerations of dropped objects, applied to the tilt shaft and payload [Kausel, 2016]

In order to develop a more reasonable test, I had to extend the time over which the impact force acted. I could achieve this by attaching a more forgiving material

of known spring constant to the bottom of the payloads, and then dropping the subsystem onto a much stiffer material such as thick steel. The material would act as a spring, slowing the impulse and allowing for a higher drop. The process to characterize the test was as follows:

1. Identify a material of known modulus of elasticity, E
2. Calculate the spring constant K from the modulus of elasticity and the area and thickness of the material, where

$$K = \frac{E * A}{H} \tag{3.2}$$

3. Solve for the natural frequency,

$$\omega_n = \sqrt{\frac{K}{m}} \tag{3.3}$$

4. Solve for the initial velocity at impact,

$$\dot{u_0} = \frac{60 * g}{-\omega_n} \tag{3.4}$$

5. Solve for the drop height using conservation of energy,

$$gh = \frac{1}{2}\dot{u_0}^2 \tag{3.5}$$

However, accelerometers are bandwidth limited, meaning the peak acceleration impulse could occur in between data points. While a laser interferometer or high-speed camera could capture such a peak, the equipment is costly and difficult to source,

and accelerometers are readily available in the laboratory. In order to fall within the bandwidth of those accelerometers, I considered various spring systems. Attaching a spring to each payload would create a measurable acceleration. The large mass of the subsystem dictated using heavy-duty coil springs, such as used in automobiles, or even leaf springs as seen in figure 3-8. While these spring systems did control the impulse time, they left unresolved the issue of maintaining a perfectly parallel drop such that both payload springs struck the contact plate simultaneously. If one spring contacted before the other, the accelerations experienced on each end would not match the objective of the test. The added time and complexity of manufacturing linear bearings and flexures to precisely control the drop test rendered this method untenable.

Figure 3-8: A single stage multi leaf spring [Akar, 2017]

Impact Testing A pendulum can easily be characterized, allowing a researcher to know the kinetic and potential energies at any point along its arc, as well as its velocity. This presented an opportunity to develop a repeatable test wherein the shaft and payload system acted as the mass, which was then released from a known angular displacement to contact a spring of known constant, inducing the desired acceleration for the shock test on the interface. However, a simple pendulum on a wire or string does not offer torsional control of the mass, and an essential component of this test was that the shaft strike perpendicular to the spring, including a bending moment at the interface to the payload. Charpy impact tests, used to determine the amount of energy absorbed by a material during fracture, offer an example of a controlled and repeatable test using a physical pendulum to contact another object.

Inspired by Charpy testing rigs, I developed a mathematical design spreadsheet

Figure 3-9: A Charpy impact test machine [NIST, 2017]

that calculated the acceleration experienced by a mass on a physical pendulum from a given angular displacement. The physical pendulum was a viable solution to create a repeatable shock test, and was selected for design and manufacture.

3.4 Development of the Reduced-Scale Shock Test

3.4.1 Requirements

The physical pendulum shock test rig needed to meet several derived requirements in order to facilitate local testing:

1. Physically small enough to be safely operated with the laboratory and easily manipulated and moved
2. Withstand the resultant forces and stresses of a low mass test interface released from up to 90 degrees angular displacement
3. A pendulum arm that prevented torsion of the test interface when released
4. A backstop to halt the pendulum arc and induce the required acceleration while maintaining alignment of the points of contact
5. Accommodate sensors, cabling, and interfaces required to capture the acceleration data

6. Controlled release of the test interface from a given angular displacement

7. Manufacturable on MIT campus with readily available materials and parts

3.4.2 Development

After considering a large pendulum rig for testing outdoors, it became clear than such an endeavor would challenge the manufacturing spaces available and would jeopardize the schedule as I was machining and assembling this rig. A smaller, local system was preferred. The optics table in the PERG laboratory was the ideal space to mount this system, as it provided a stable surface with mounting holes that could secure the pendulum rig from moving during testing. This space limited the pendulum arm to little more than 1.3 meters.

With the critical dimension of the pendulum arm determined I developed free body diagrams illustrating the forces experienced by the shock rig during testing from maximum angles, such as that seen in figure 3-10. These forces did not exceed

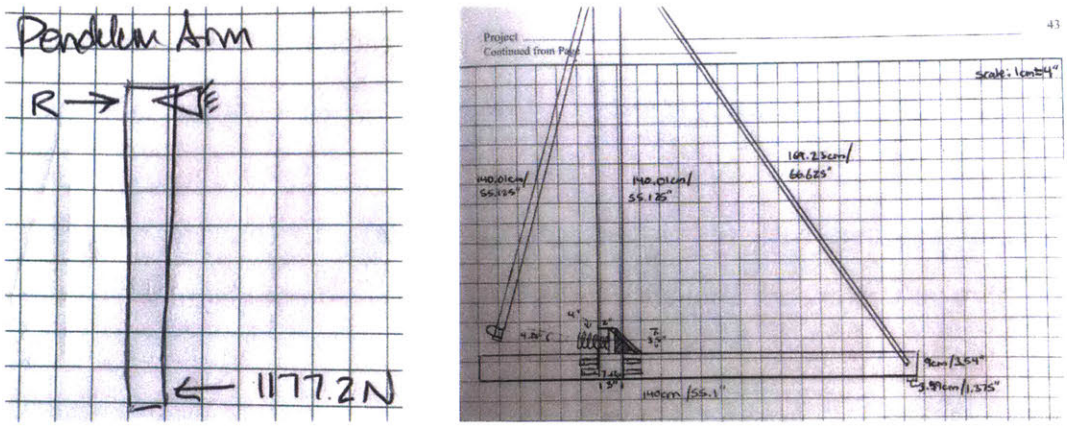

Figure 3-10: Free body diagram and sketch of shock pendulum concept

the specifications of the 80-20 T-slotted aluminum framing in the laboratory and ubiquitous in experimental structures. In order to minimize the moments on the

bolted joints of the structure, I minimized the width of the pendulum support structure, choosing to connect the uprights supporting the arm, and all other structural members, to a single large beam that would, in turn, be mounted to the optics table.

6061 aluminum square tubing was selected for the pendulum arm in order to maintain a low mass while ensuring alignment of the test interface and contact point by prohibiting twisting during travel. The tubing was treated as a simply supported beam, conservatively point loaded in the center at the time of impact. These calculations ensured that the pendulum arm would not fail or deform during maximum acceleration testing. The pendulum arm needed to be securely fastened to the pivot shaft. Circumferential clamps provide very good torque transmission, low stress concentration, and are easily milled [Slocum, 2008]. For this component attachment, a split-housing circumferential clamp ensured nearly continuous contact between the square tubing of the pendulum arm and the pivot shaft, which was sized to the inner dimension of the tubing. The pivot shaft itself was secured to minimize deflections utilizing Saint-Venant's principle, which states that "several characteristic dimensions away from an effect, the effect is essentially dissipated." Maxwell's reciprocity then suggests that an effect will dominate a system when applied over three to five characteristic dimensions of a system [Slocum, 2008]. The pivot shaft bearings with positioned accordingly, ensuring that the bearings would effectively resist moments applied to the shaft. I specified self-aligning bearings rated to withstand the calculated testing forces.

I considered attaching the spring to the swinging test subject but determined that machining it into the backstop at the bottom of the arc would simplify the manufacturing process and avoid potential inconsistency between test subjects, as only one mount would be required. The spring could have been in the forms discussed

previously as leaf springs, coils, or Belleville washer. Knowing that

$$I\frac{d^2\theta}{dt^2} + (\frac{L}{2}m_{arm}g + Lm_{test}g)sin(\theta) = 0 \tag{3.6}$$

and that the kinetic energy of a physical pendulum is

$$KE_{pp} = \frac{1}{2}I(\frac{d^2\theta}{dt^2})^2 \tag{3.7}$$

and assuming no losses, I was able to determine the energy transfered into the spring. This provided the displacement of the spring, from which the force and then acceleration could be determined. The calculated displacements and the complexity of mounting a leaf spring or Belleville washer directed the use of a tempered steel jumbo compression spring.

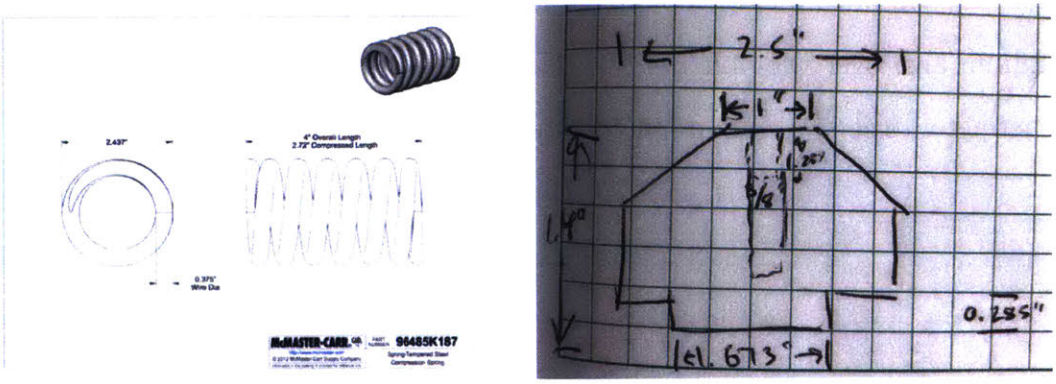

Figure 3-11: Shock test compression spring and cap for tooling ball [McMaster-Carr, 2017]

Furthermore, each of these spring mechanisms presented a large contact area. The compression spring, with closed and ground flat ends, provided a means to mount a Hertzian contact point that would eliminate errors from minor misalignment. This was accomplished by machining a tapered cap that was mounted to the compression

spring, into which a steel tooling ball was inserted. Using a Hertzian contact design spreadsheet [Slocum, 2011], I determined that the contact at maximum acceleration would induce yielding in the aluminum of the pendulum arm. While repeated contact yielding would lead to a cold-formed spherical pocket upon repetition, I wanted to eliminate the possibility of unaccounted travel distance during spring compression. The test model mount required a bolt through the pendulum arm, so I located this bolt to be the contact point. The bolt head, also steel, would not deform from the Hertzian contact stresses.

In order to ensure accurate data on the acceleration of the test piece, the pendulum arm had to accommodate sensors aligned with the interface model and the point of contact. The mount also needed to be stiff in the direction of the acceleration to prevent the accelerometers from experiencing different accelerations than the test model. A simple bracket mount located the accelerometers directly behind the pendulum arm over the bolt used to both secure the test model and as the point of contact to the spring-mounted tooling ball as seen in figure 3-12. This sensor platform was large enough to accommodate multiple sensors simultaneously for calibration and comparison while setting up the initial experiment to validate the testing model. From this sensor platform I ran the cabling up the pendulum arm to the pivot, securing the cables with enough slack to account for all angular displacements before connecting the cables to the sensor interface mounted on an upright.

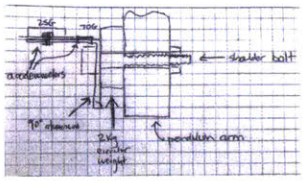

Figure 3-12: Sensor mount concept sketch

The arm of the shock test rig needed to be released from a consistent angular displacement for each test, which required a release mechanism. Drop tests often incorporate electronic release systems. The shipping industry has informed the development of release hooks designed for massive systems, specified up to thousands of pounds

[IDM, 2013]. These systems are expensive and require power connections to operate. Always seeking simplicity and a tie-in the nautical nature of this project, I decided to use a quick-release knot that can be untied under tension with a simple tug on the bitter end. The tumble hitch, seen in figure 3-13 is the most stable variation of the highwayman's hitch, securely supporting large loads without jamming when released.

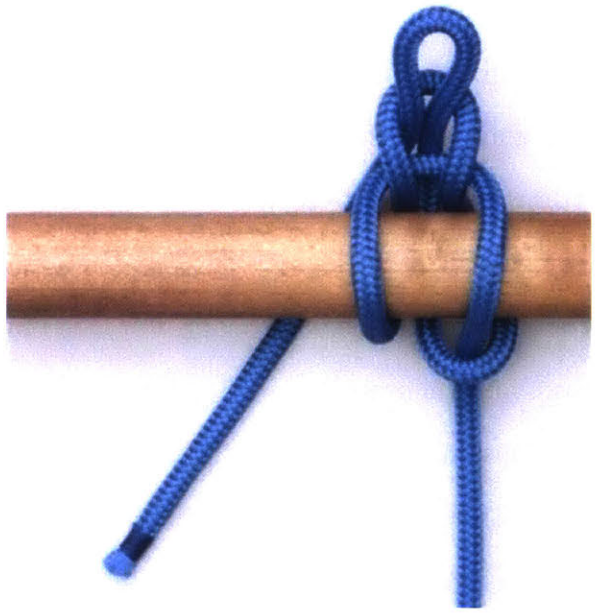

Figure 3-13: A tumble hitch [AnimatedKnots, 2016]

3.4.3 Manufacturing

All of the machined components of the shock testing rig were made of aluminum. The base was a 80-20 aluminum slotted beam measuring 9 *cm* by 9 *cm*, to which two 140 *cm* tall uprights were attached on either side with four brackets each. I drilled through the base beam and two pieces of 170 *cm* long aluminum angle stock to create triangular supportive brackets for the uprights, spaced using spare 80-20 slotted stock. The uprights were also connected by the 3/4 inch pivot shaft, which ran between a mounted ball bearing with cast iron housing on each upright. Those

bearings, as the brackets, were attached by end-feed fasteners in the T-slots. I milled a matching hole for the shaft in the top of the pendulum arm and a smaller 1/2 inch bolt hole above and orthogonal to that hole, then split the square tubing using a slot cutter on the mill to create a circumferential clamp. On the mass end of the pendulum arm I milled a 3/4 hole for a bolt to mount the test interface model, sensor platform, and act as the contact point. The sensor platform was an aluminum 90° angle stock into which I milled holes for the mounting bolt and each of the sensor connection bolts (10-32 and 4-40 screws requiring #7 and #30 drill bits for the 25 and 70 g-force accelerometers, respectively).

The coil spring needed a block into which it could be mounted and then attached to the double bracket securing it to the base beam. For this I faced a 2 *in* by 3.5 *in* by 2.5 *in* block of aluminum and then used a CNC mill to bore a 2.437 *in* diameter blind hole into which the spring could be mounted. I drilled and tapped the back of the block so that it could be attached to the double bracket using four 1/4-20 bolts. The final component was the tapered cap to hold the tooling ball and create the Hertzian contact point. I faced a 1.5 *in* long section of 2.5 *in* diameter aluminum bar stock, then used the lathe to create a boss matching the coil spring inner diameter at 1.687 *in*. The lathe taper function facilitated tapering to the 1 *in* diameter tooling ball face, into which I drilled a 1.25 *in* deep blind hole using a 25/64 drill bit to ensure a press fit. Once this was mounted, the machine was ready for testing with a control mass that would simulate the interface test model and validate the calculated relationship between mass, angular displacement of the pendulum arm, and acceleration upon contact with the spring.

3.5 Designing the Reduced-Scale Interface

3.5.1 Computer Modeling

The first iteration of the reduced-scale design was a shortened shaft and a cup-like flange designed to hold standard lifting weights on the end to permit testing at various payload masses. The center of the shaft was machined flat to sit flush on the pendulum arm, and the sides of that flat served to prevent twisting. In order to increase the mass of the flange/payload pieces and simplify manufacturing, I worked with Professor Slocum to design a more robust small shaft featuring chamfers instead of fillets wherever possible, and increased the flanges to hold Olympics weights.

Figure 3-14: Exploded isometric view of the reduced-scale model

3.5.2 Manufacturing

The model was sent out for quotes and the manufacturing contract awarded to Startsomething LLC. During the quote process, I received feedback on the drawings and requests for clarification on the design, such as the surface finish requirement and

any tolerances. This was an important learning point for the future, full-scale design, for which tolerances and finishes were critical.

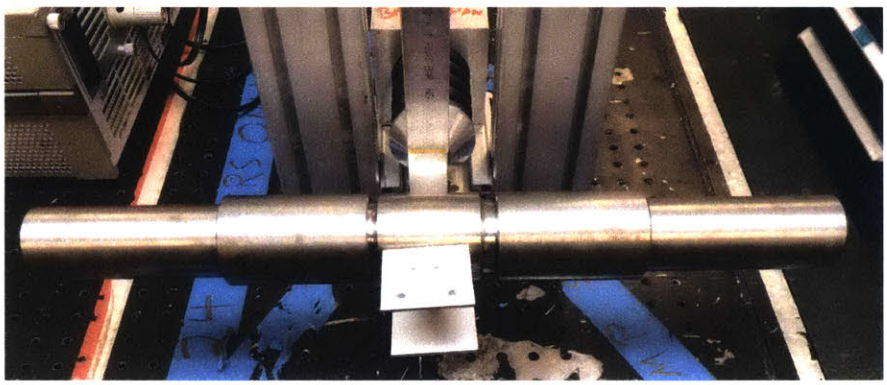

Figure 3-15: Reduced scale model mounted to the pendulum rig

3.6 Development of the Full-Scale Shock Test

The full scale prototype of the interface design required a test using the payload models provided by the NRL, at a mass of 38.55 kg each. The laboratory shock rig was not designed to accommodate these forces, compelling me to develop a second shock test. Returning to the concept of a drop test, I examined the potential of utilizing the full scale model shaft and a simply-supported beam as springs in series to control the impulse.

3.6.1 Requirements

In order to facilitate local testing the drop test needed:

1. to be physically small enough to be moved into and safely operated within a campus space.

2. to withstand the resultant forces and stresses of a nearly 80 kg subsystem experiencing 60 g-forces.

3. to accommodate sensors, cabling, and interfaces required to capture the acceleration data.

4. a controlled release of the test model.

5. to be manufactured on MIT campus with readily available materials and parts.

3.6.2 Development

A testing solution to ensure the precise alignment concern was to drop the shaft and payload subsystem onto a simply supported cylindrical beam such that the shaft being tested contacted the supported beam. The simply supported beam acted as a spring where

$$K = \frac{48EI}{L^3} \tag{3.8}$$

and the tilt shaft behaved as a beam cantilevered from the point of contact, which is a spring where

$$K = \frac{3EI}{(\frac{L}{2})^3}. \tag{3.9}$$

Treating these as springs acting in series, I solved for an equivalent spring constant where

$$\frac{1}{K_{eq}} = \frac{1}{K_{ss}} + \frac{1}{K_{shaft}} \tag{3.10}$$

and determine the height from which to drop the shaft and payloads. This method permitted large spring constants that made it a viable candidate for testing the full scale interface from a drop height that did not exceed the length of the accelerometer cables.

Both the simply supported beam and the shaft containing the developed interface needed to withstand the stress of the impact without plastic deformation or failure. The maximum flexural stress in a beam of symmetric cross-section can be calculated using the equation

$$\sigma_{max} = \frac{Mc}{I} \tag{3.11}$$

where M is the applied moment, I is the moment of inertia of the cross-sectional area, and c is the maximum distance from the neutral axis - in this case, the radius. The maximum shear stress in a beam of circular cross-section is given by

$$\tau_{max} = \frac{4V}{3A} \tag{3.12}$$

where V is the shear force and A is the cross-sectional area of the beam. These stresses were calculated for the interface shaft and compared to the yield and shear yield stresses for 1018 steel. In order to ensure the strength of the test shaft, I determined to keep it solid through testing, after which it could be hollowed for the required control cabling and installed in the prototype pan-tilt machine. The stresses for the simply supported spring beam were calculated and compared similarly in a custom design spreadsheet, using the Von Mises stress to ensure the material would not yield during testing. The Hertzian contact stresses experienced by the two shafts in contact were calculated using the Hertzian contact design spreadsheet to confirm that the shafts would not deform. Finally, I calculated the stress at the pin of the simple support to verify that it would not shear, nor would it cause failure of the beam at the joint.

The sensors now had to be attached to the payloads. This was achieved by tapping the payloads for 10-32 and 4-40 screws to mount the 25 and 70 g-force accelerometers,

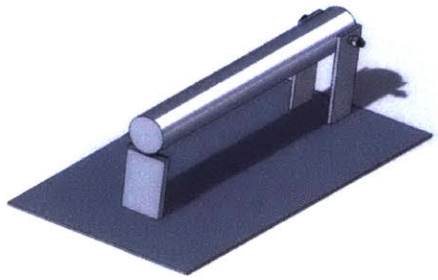

Figure 3-16: Simply-supported beam for full scale test

respectively. The cabling ran clear of the drop area. As with the pendulum shock rig, a tumble hitch provided a controlled release. Because two cylindrical shafts were colliding at a Hertzian contact point, the acceleration experienced by the payloads was not affected if the tilt shaft was not parallel to the ground at contact.

3.6.3 Manufacturing

The beam was turned from steel round bar stock. Two upright steel supports were welded to a base plate, on which a third support was placed orthogonal to the first two. The beam was pinned between the parallel supports and allowed to rest on the orthogonal support as seen in figure 3-16. This simply supported structure was then placed beneath a shop crane that was used to hold the shaft and payload subsystem. The interface was raised to the appropriate height for the test.

3.7 Designing the Full-Scale Interface

3.7.1 Computer Modeling

This model was designed to meet the existing tilt shaft housing parameters, and thus was partially geometrically defined, such as in diameter where the bearings sit.

Figure 3-17: Full scale shock test setup

Taking advantage of the additional resistance afforded by the hollowed bolt, and the ability to increase the pre-load if desired, I reduced the engagement length of the interface to decrease the footprint of the gimbal. To compensate for this reduction in engagement length, I reduced the taper angle as well. As discussed, the model for testing was not hollow throughout to prevent damage when point loaded at the midpoint of the beam, something that will not happen in the gimbal. The drop test model also did not include any external features, such as the elevation hard stop or the cable entry. Figure 3-18 shows the version as ready for use in the gimbal.

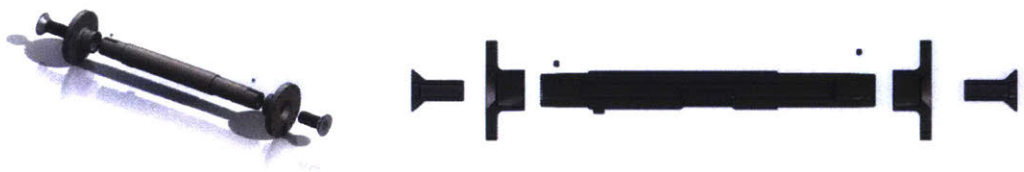

Figure 3-18: Exploded isometric and cross-section views of the tilt shaft and payload interface design

3.7.2 Manufacturing

The model was manufactured by the MIT Central Machine Shop over the course of a week. The shaft taper and flange taper were completed to a 16 surface finish and tested with engineer's blue to ensure complete contact throughout.

THIS PAGE INTENTIONALLY LEFT BLANK

Chapter 4

Results

4.1 Pendulum Rig Validation Results

I tested the pendulum rig using a known mass in order to characterize the system for conducting future tests. I conducted five swings at ten degree intervals between ten and seventy degrees. The first data collected was noisy from the vibrations of the pendulum arm, so I added material as a damper with two sided tape as seen in figure 4-1.

Figure 4-1: Damped pendulum arm

I used a moving average to filter the data. A moving average depends upon the window size used. I determined the maximum window size from the impulse time of the shock test, selecting as many points at 10 kHz sampling rate would fit into that period. In order to determine the window size choice, I used the code in appendix C to plot the sum of absolute differences between the filtered and raw data over every window size up to the predetermined maximum. Where

the curve steadied was the window size used. An example of this, performed on the tests at twenty degrees, is seen in figure 4-2.

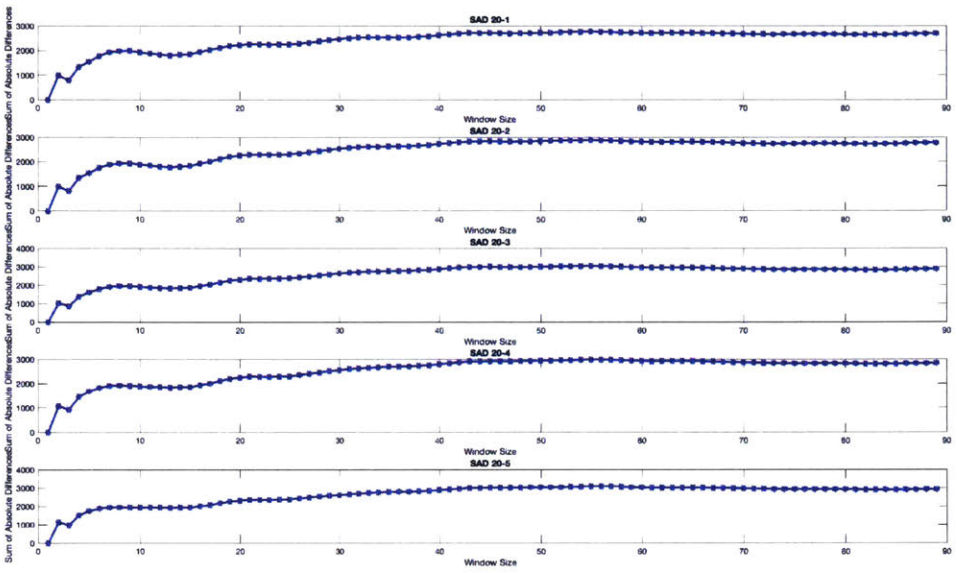

Figure 4-2: Determining window size using SAD at 20 degrees

After filtering the data, I was able to determine the peak acceleration for each swing at each angle. These, in turn, were analyzed in a normal distribution to determine the average and the 95% confidence interval of the results. Finally, the averages were plotted over each angle with a best-fit curve as seen in figure 4-3.

The pendulum rig was successful in delivering the required smaller shocks necessary to test the reduced-scale model. Even with the added damping and bolting the system in place there was substantial vibration and noise. A future design should explore a more stiff pendulum arm and increased lateral support for the pivot point of the pendulum.

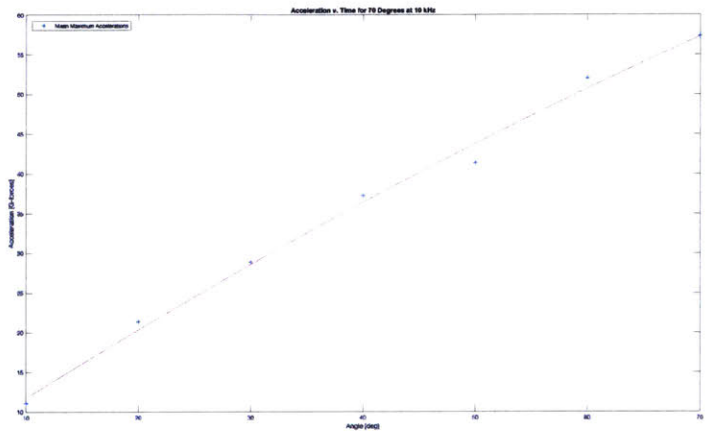

Figure 4-3: Test mass results for the pendulum shock rig

4.2 Reduced-Scale Shock Test Results

After thus validating the pendulum, I tested the reduced-scale model. The push-on force was calculated such that the interface would "fail" when subjected to a 20 g-forces acceleration, meaning that the flange would come loose from the shaft. The flanges were pressed onto the shaft, and the bolts backed out partly to permit movement while securing the flanges from leaving the test rig entirely.

During the first tests, the model did not "fail" as predicted. I returned first to the push-on force calculations, iterating them to a very low push on force (and thus very low required torque to apply – too low, in fact, for the wrenches available). I used a force gauge to push on the flanges with ever lower forces, finally inducing failure on a swing. Returning to the MATLAB code, the source of the error became obvious immediately. The distance used to calculate the bending moment of the payload at impact had not been scaled down to match the test shaft and flange dimensions, and thus was predicted to be much larger than actually experienced during testing.

I corrected the MATLAB code moment arm inputs, and proofed the code for other errors. Running the code again predicted failure at 20 g-forces using the same

push-on force originally desired. I secured the flanges, marked the intersection of the flange ends and the shaft, and then backed the screws out several turns so that any loosening would be readily apparent but would prevent the flanges from departing the shaft entirely. This test proved successful, suggesting that the math was correct and that a larger scale design was feasible.

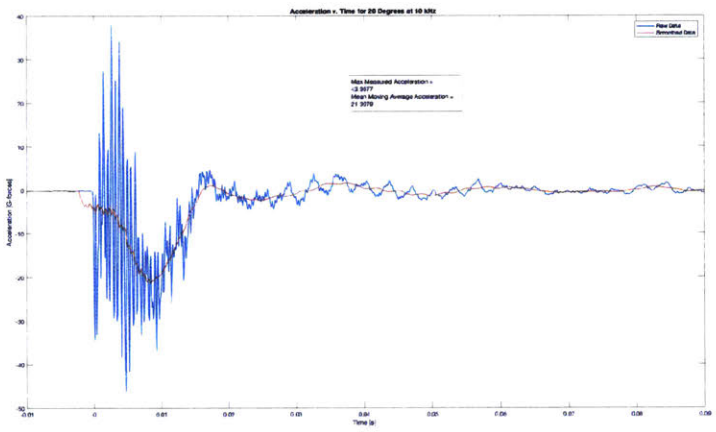

Figure 4-4: Acceleration plot from 20 degree test

4.3 Full-Scale Shock Test Results

The full scale drop test used both a 70 and a 500 g-force accelerometer. As the results rapidly exceeded 70 g-forces, the data presented here is only that from the 500 g-force sensor. Additionally, the 70 g-force sensor cable severed during the third test, rendering it unusable for the last two tests.

The data collected from the full-scale drop test was significantly less noisy than the pendulum rig data. The impulse time contained approximately 26 data points, and the peaks of the 500 g-force accelerometer results comprised upwards of 17 points, indicating reliable maximum value data. For comparison, I still plotted a moving

average of the data using the window size dictated by comparing the sum of absolute differences to the window size. This analysis can be found in appendix D.

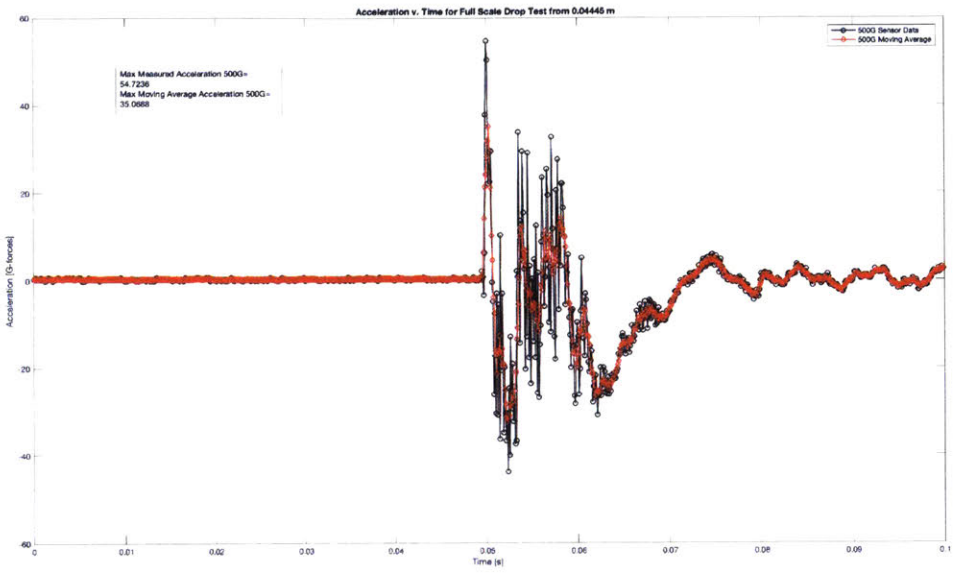

Figure 4-5: Test 1

4.4 Conclusion

This tapered interface successfully met the requirements for the gimbal and may be utilized in the prototype machine. It reduces the part count and the time required for maintenance and repair. It could be further reduced in size, but that would require an increase in pre-load and thus application torque. This design proves that tapers are a feasible method to connect massive loads to their actuators, and can use different geometry than established in automotive and marine industries. There is potential to use this technology with large actuators in industry. Future work on this project could include making a graphic user interface for the code such that a designer could input some parameters and have a taper design iterated from the code.

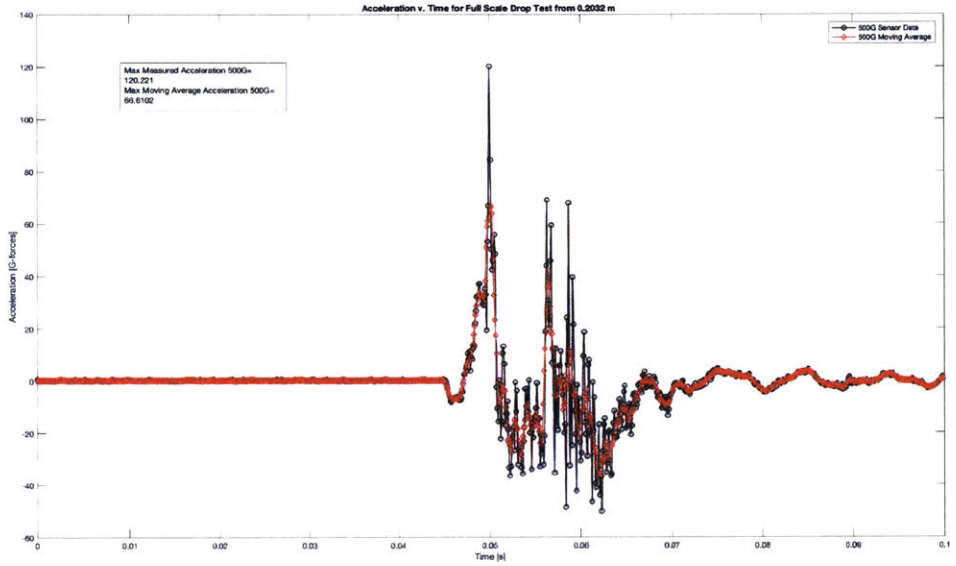

Figure 4-6: Test 2

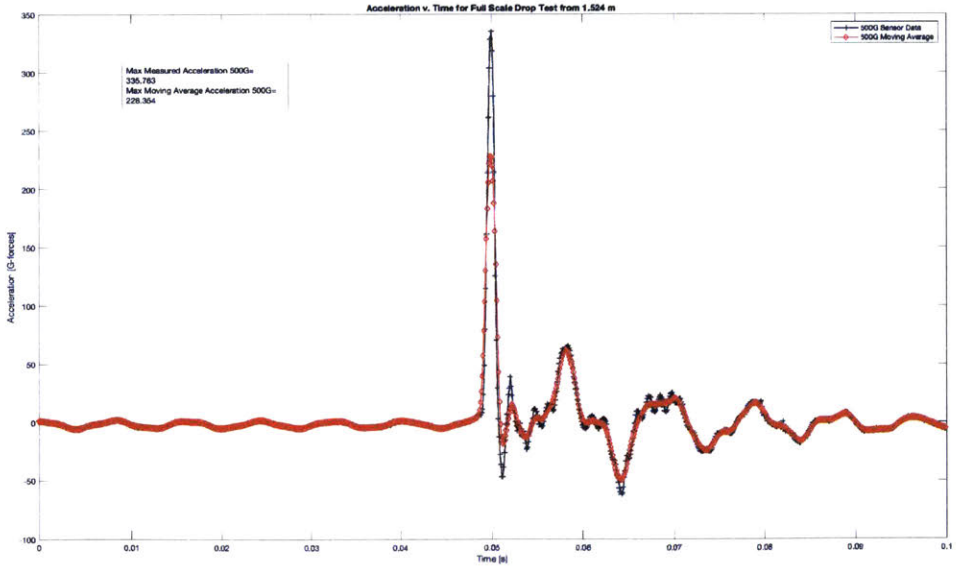

Figure 4-7: Test 3

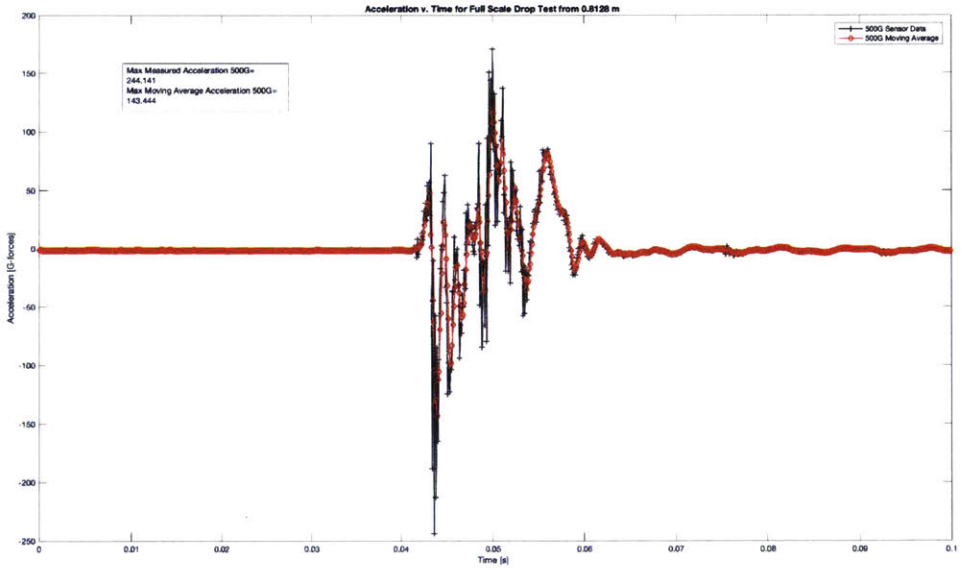

Figure 4-8: Test 4

THIS PAGE INTENTIONALLY LEFT BLANK

Appendix A

Hand Calculations

I calculated the taper retaining moment and that of a cylinder with only 30 degrees of contact on either side to see how the two compared. Those calculations are shown in figures A-1 and A-2, respectively.

20 Project Tilt shaft Payload Interface

Continued from Page

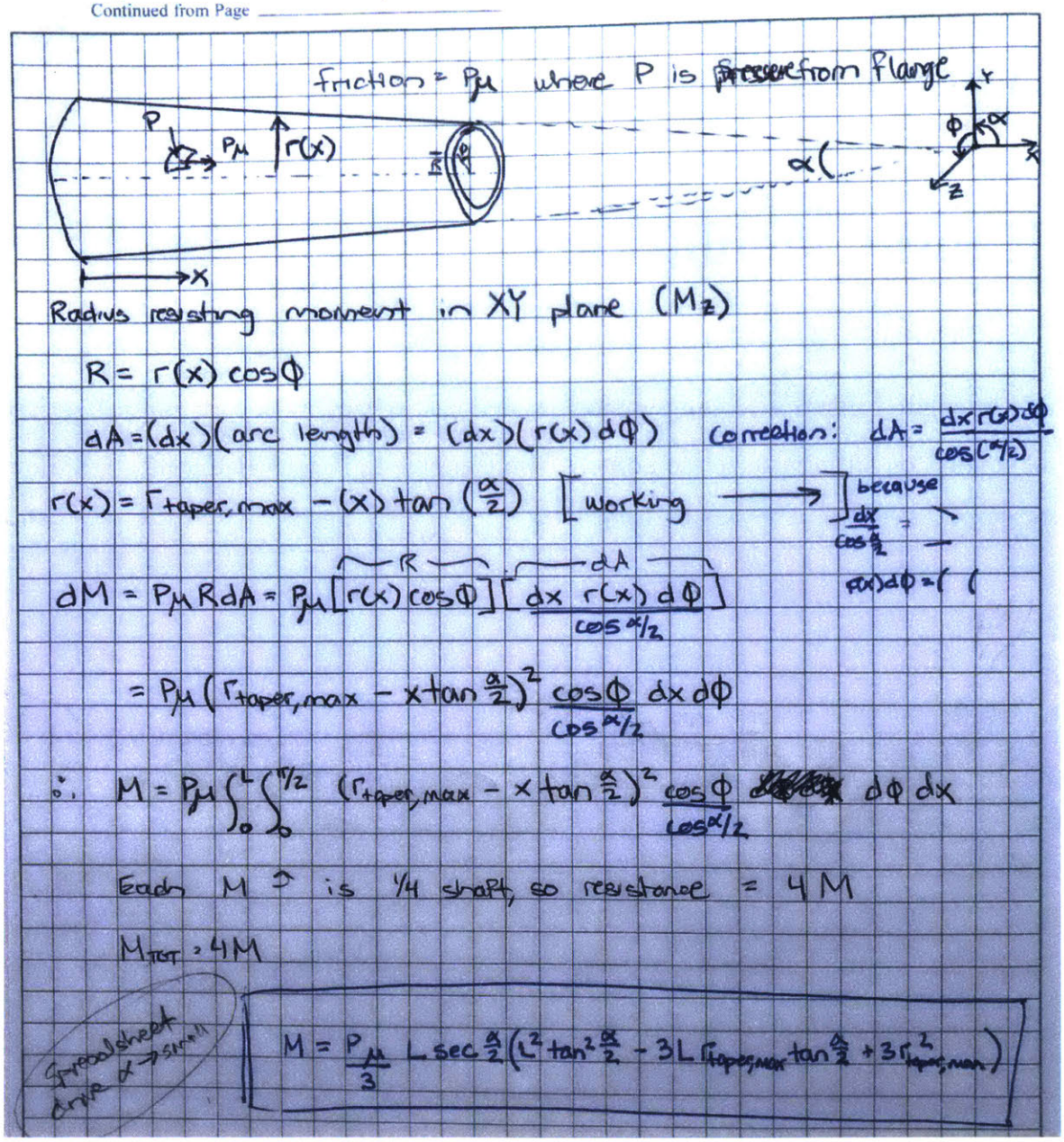

Figure A-1: Taper Calculations

Project Tilt Shaft Payload Interface 21

Continued from Page 20

P is a function of the max assembly force over the area of the frustrums (see ME Ref Manual p53 56)

L is function of current tilt housing dimensions and max payload width anticipated to reduce weight and footprint.

μ From dry assemblies in ME Ref Manual 53.9

Diameters will be informed by Timken bearing sizes for tilt shaft, and torsional shear / wall thickness

MATLAB results must compare w/ intuition @ 30° contact

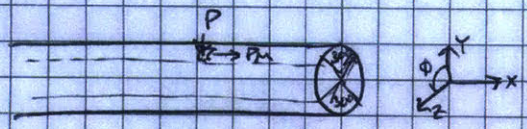

$R = r\cos\phi$ (constant r) $\quad dA = r\,d\theta\,dx$

$$M = P_\mu \int_0^L \int_{-\pi/12}^{\pi/12} r^2 \cos\phi \, d\phi \, dx = P_\mu \int_0^L \frac{(\sqrt{3}-1)r^2}{\sqrt{2}} \, dx$$

$M_{TOT} = 2M$ (top and bottom acting together)

Results match approximately $\quad P = 2.7 \times 10^7 \ N/M^2$

$F_A = 4.09 \times 10^4 \ N$

$$\boxed{M = P_\mu L r^2 \left(\frac{\sqrt{3}-1}{\sqrt{2}}\right)}$$

Continued on Page

Figure A-2: Cylinder Calculations for 30 Degrees Contact

THIS PAGE INTENTIONALLY LEFT BLANK

Appendix B

Interface Mathematical Model

```
%%%%%%%%%%%%%%%%%%%%%%%%%%%%%%%%%%%%%%%%%%%%%%%%%%%%%%%%%%%%%%%%%%%%%%%%%%%%%%%
% This code determines the interface's ability to withstand all
% loading and force requirements, as well validating that the shaft,
% flange, and screw will not fail materially in the process.
%%%%%%%%%%%%%%%%%%%%%%%%%%%%%%%%%%%%%%%%%%%%%%%%%%%%%%%%%%%%%%%%%%%%%%%%%%%%%%%

clf
close all
clear all
clc


%%%%%%%%%%%%%%%%%%%%%%%%%%%%%%%%%%%%%%%
% Physical Contraints
%%%%%%%%%%%%%%%%%%%%%%%%%%%%%%%%%%%%%%%

g=9.81;              %gravity [m/s^2]
```

```
18
19 E=200E9;              %Young's Modulus of AISI 4340 Stainless Steel [Pa]
20 nu=0.29;             %Poisson's Ratio of AISI 4340 Stainless Steel
21 rho=7850;            %Density of AISI 4340 Stainless Steel [kg/m^3]
22 sigma_yield=972E6;   %Tensile Yield tSrength of AISI 4340 SS [Pa]
23
24 mu=0.213650328; %measured coefficient of friction for flange and shaft [Pa]
25
26 %tensile strength of screw [Pa]
27 screw_tensile=convpres(120000, 'psi', 'Pa');
28
29 %shear yield stress of screw per Shigley Eqn 5-21 [Pa]
30 screw_shear=0.577*screw_tensile;
31
32
33 %%%%%%%%%%%%%%%%%%%%%%%%%%%%%%%%%%%%%%%%
34 % Requirements
35 %%%%%%%%%%%%%%%%%%%%%%%%%%%%%%%%%%%%%%%%
36
37 shock=60*g;                  %shock requirement [m/s^2]
38
39 %max angular velocity [rad/s]
40 omega_req_max=convangvel(100, 'deg/s', 'rad/s');
41
42 %max angular acceleration [rad/s^2]
43 alpha_req_max=convangacc(100, 'deg/s^2', 'rad/s^2');
44
45 d_tilt_inner=0.020;          %clearance for control cabling [m]
46 r_tilt_inner=d_tilt_inner/2;     %clearance for control cabling [m]
47
48
```

```
%%%%%%%%%%%%%%%%%%%%%%%%%%%%%%%%%%%%%%%%
% Tilt Shaft and Payload Dimensions
%%%%%%%%%%%%%%%%%%%%%%%%%%%%%%%%%%%%%%%%

%PAYLOAD
m_payload=77.1107/2;     %mass of each payload [kg]
LCG_payload=0.2;         %distance to center of gravity of payload [m]

%TILT SHAFT
d_tilt=0.05;            %large end diameter of tilt shaft to fit bearing [m]
r_tilt=d_tilt/2;        %large end radius of tilt shaft [m]

%TILT FLANGE AND HOUSING
t_r=0.013;               %retainer thickness [m]
t_b=0.016;               %tilt shaft bearing thickness [m]
L_offset=0.002;          %prevents flange from exceeding taper [m]

t_flange=0.015;          %flange vertical thickness [m]
d_flange_outer=0.05988; %outer diameter of flange hub on taper [m]
r_flange_outer=d_flange_outer/2;    %outer radius of flange hub on taper [m]
chamfer_flange=0.002;    %chamfer [m]

%FLANGE SCREW
%pitch diameter of 1 1/4-12 3A screw [m]
d_m_bolt=convlength(1.1959, 'in', 'm');

%minor diameter of 1 1/4-12 3A screw [m]
d_minor_bolt=convlength(1.1508, 'in', 'm');
r_minor_bolt=d_minor_bolt/2;         %minor radius of 1 1/4-12 3A screw [m]
lead=convlength(1/12, 'in', 'm');    %inverse of threads per inch [m]
thread_angle=60;                     %UNC thread angle [degrees]
```

```
80
81 %flange screw average collar diameter [m]
82 d_c=convlength((2.438+1.25)/2, 'in', 'm');
83 screw_length=convlength(3, 'in', 'm');      %screw length [m]
84
85 screw_thread_length=convlength(3-.683, 'in', 'm');  %threaded length [m]
86 screw_head_height=convlength(0.683, 'in', 'm');   %head height of screw [m]
87 screw_head_diameter=convlength(2.438,'in','m'); %diameter of screw head [m]
88
89 %%%%%%%%%%%%%%%%%%%%%%%%%%%%%%%%%%%%%%%%
90 % Shepstone Taper Input Variables
91 %%%%%%%%%%%%%%%%%%%%%%%%%%%%%%%%%%%%%%%%
92
93 M_a=m_payload*shock;     %thrust of axial shock on payload [N]
94 t=16;                     %inverse of shaft taper
95 L_interface=.038;        %length of interface between flange and shaft [m]
96
97 %distance from tilt shaft bearing to payload center of gravity [m]
98 L_moment=(.5*t_b) + t_r + L_offset + L_interface + t_flange + LCG_payload;
99
100
101 %%%%%%%%%%%%%%%%%%%%%%%%%%%%%%%%%%%%%%%%
102 % Shepstone Taper Calculated Variables
103 %%%%%%%%%%%%%%%%%%%%%%%%%%%%%%%%%%%%%%%%
104
105 c_tilt_min=1/t;      %shaft taper (diameter to length)
106
107 %taper angle from edge to shaft centerline [deg]
108 taper_angle=atand(1/(2*t));
109
110 d_a=d_tilt-(L_interface*c_tilt_min);     %small end diameter tilt shaft [m]
```

```
111 d_m=d_tilt-(L_interface/(2*t));          %mean shaft diameter [m]
112
113 %max radius of shaft taper contacting flange [m]
114 r_tilt_taper_max=(d_tilt/2)-chamfer_flange*tand(taper_angle);
115 r_tilt_taper_min=d_a/2;
116
117 % Shepstone Quadratic Equation Constants [non-dimensional]
118 a=(mu^2)*cosd(taper_angle)^2-sind(taper_angle)^2;
119 b=-(mu^2+1)*2*M_a*cosd(taper_angle)*sind(taper_angle);
120 c_tilt_min=(mu*M_a*sind(taper_angle))^2-(M_a*cosd(taper_angle))^2;
121
122 %required radial force to prevent slip for axial thrust [N]
123 M_i=(-b+sqrt(b^2-4*a*c_tilt_min))/(2*a);
124
125 area=pi*L_interface*d_m;     %contact area of flange and shaft [m^2]
126
127 p=M_i/area;                  %required average interface pressure [Pa]
128
129 %required push on force [N]
130 F_d=M_i*(sind(taper_angle)+mu*cosd(taper_angle))/...
131     (cosd(taper_angle)-mu*sind(taper_angle));
132
133
134 %%%%%%%%%%%%%%%%%%%%%%%%%%%%%%%%%%%%%%%%%%%%%%%%%%%%%%%%%%%%
135 % Calculate Screw Torque with Shigley Equation 8-25a
136 %%%%%%%%%%%%%%%%%%%%%%%%%%%%%%%%%%%%%%%%%%%%%%%%%%%%%%%%%%%%
137
138 Torque=(F_d*d_m_bolt/2)*((lead+pi*mu*d_m_bolt*secd(thread_angle))...
139     /(pi*d_m_bolt-mu*lead*secd(thread_angle)))+(F_d*mu*d_c/2);% [N*m]
140
141
```

```
%%%%%%%%%%%%%%%%%%%%%%%%%%%%%%%%%%%%%%%%%%%%%%%%%%%%%%%%%%%%%%%%%%%%%%%
% Check that screw and internal threads will not yield
%%%%%%%%%%%%%%%%%%%%%%%%%%%%%%%%%%%%%%%%%%%%%%%%%%%%%%%%%%%%%%%%%%%%%%%

n_t=screw_thread_length/lead;    %number of threads engaged on screw (all)

%minimum major diameter of internal threads [m]
d_internal_thread=convlength(1.25, 'in', 'm');

%cross-sectional area through which internal thread shear occurs calculated
%from Fastenal Engineering and Design Support "Screw Thread Design"
%document using INCH units to match the equation. 12 is the threads per
%inch, 3 is the engagement length, 1.2386 is the minimum major diameter of
%external threads from efunda, 1.2019 is the maximum pitch diameter of the
%internal threads [in^2]
area_internal_threads=pi*12*3*1.2386*((1/(2*12))+0.57735*(1.2386-1.2019));

%convert cross-sectional area of internal threads to metric [m^2]
area_internal_threads=area_internal_threads*convlength(1, 'in', 'm')^2;

%axial stress in screw per Shigley Eqn 8-8 [Pa]
axial_stress_screw=F_d/(pi*(r_minor_bolt^2-r_tilt_inner^2));

%bending stress at root of thread per Shigley Eqn 8-11 [Pa]
bending_stress_screw=(6*F_d)/(pi*d_minor_bolt*n_t*lead);

%transverse shear stress at center of thread root per Shigley Eqn 8-12 [Pa]
shear_screw_thread=(3*F_d)/(pi*d_minor_bolt*n_t*lead);

%shear stress at internal thread per Fastenal Eng & Design Support [Pa]
shear_internal=F_d/area_internal_threads;
```

```
173
174 if axial_stress_screw>screw_tensile || bending_stress_screw>screw_tensile...
175         || shear_screw_thread>screw_shear || shear_internal>screw_shear
176     display('Screw will not provide pre-load.')
177 else display('Screw will provide pre-load.')
178 end
179
180
181 %%%%%%%%%%%%%%%%%%%%%%%%%%%%%%%%%%%%%%%%%%%%
182 % Check that taper will transmit torque
183 %%%%%%%%%%%%%%%%%%%%%%%%%%%%%%%%%%%%%%%%%%%%
184
185 Ixx=484265.17;      %from SolidWorks mass properties [lbm*mm^2]
186 Ixx=Ixx*convmass(1, 'lbm', 'kg')*(1/1000)^2;    %convert to metric [kg*m^2]
187
188 Torque_tilt=Ixx*alpha_req_max;   %max torque required [N*m]
189
190 if M_i*d_m<Torque_tilt
191     display('Taper will not transmit actuating torque.')
192 else display('Taper will transmit actuating torque.')
193 end
194
195
196 %%%%%%%%%%%%%%%%%%%%%%%%%%%%%%%%%%%%%%%%%%%%%%%%%%%%%%%%%%%%%%%%
197 % Check that centripetal force will not unseat payload
198 %%%%%%%%%%%%%%%%%%%%%%%%%%%%%%%%%%%%%%%%%%%%%%%%%%%%%%%%%%%%%%%%
199
200 %centripetal force at payload LCG [N]
201 F_centripetal=m_payload*L_moment*(omega_req_max^2);
202
203 if F_centripetal>M_a
```

```
204     display('Taper will be unseated by centripetal force.')
205 else display('Taper will withstand centripetal force.')
206 end
207
208
209 %%%%%%%%%%%%%%%%%%%%%%%%%%%%%%%%%%%%%%%%%%%%%%%%%%%%%%%%%%%%%%%%
210 % Check that shock bending moment will not unseat payload
211 %%%%%%%%%%%%%%%%%%%%%%%%%%%%%%%%%%%%%%%%%%%%%%%%%%%%%%%%%%%%%%%%
212
213 M_shock=m_payload*L_moment*shock;   %bending moment due to shock [N*m]
214
215 %taper retaining moment per integration in design notebook p.20 [N*m]
216 M_taper_hold=4*((p*mu)/3)*L_interface*secd(taper_angle)*(L_interface^2*...
217     (tand(taper_angle))^2-3*L_interface*r_tilt_taper_max*...
218     tand(taper_angle)+3*r_tilt_taper_max^2);
219
220 M_total_hold=abs(M_taper_hold)+(screw_tensile*(pi*(r_minor_bolt^2-...
221     r_tilt_inner^2))*d_c);
222
223 if M_shock>M_total_hold
224    display('Taper will not hold shock moment.')
225 else
226    display('Taper will hold shock moment.')
227 end
228
229
230 %%%%%%%%%%%%%%%%%%%%%%%%%%%%%%%%%%%%%%%%%%%%%%%%%%%%%%%%%%%%%%%%
231 % Check that large diameter of taper will not yield
232 %%%%%%%%%%%%%%%%%%%%%%%%%%%%%%%%%%%%%%%%%%%%%%%%%%%%%%%%%%%%%%%%
233
234 % Centroidal Moment of Inertia for Hollow Shaft [m^4]
```

```
I_x=(pi/64)*(r_tilt_taper_max^4-r_tilt_inner^4);

M_stress=m_payload*g*L_moment;              %bending moment [N*m]
c_d_tilt=r_tilt_taper_max;                  %distance to neutral axis [m]

circum_stress_d_tilt=-((r_tilt_taper_max^2+r_tilt_inner^2)*p)/...
    (r_tilt_taper_max^2-r_tilt_inner^2);    %circumfrential stress [Pa]
radial_stress_d_tilt=-p;                    %radial stress [Pa]
bend_stress_d_tilt=M_stress*c_d_tilt/I_x;   %bending stress [Pa]

if bend_stress_d_tilt>sigma_yield || circum_stress_d_tilt>sigma_yield ||...
        radial_stress_d_tilt>sigma_yield
    display('Tilt shaft will yield at large end of taper.')
else display('Tilt shaft will not yield at large end of taper.')
end


%%%%%%%%%%%%%%%%%%%%%%%%%%%%%%%%%%%%%%%%%%%%%%%%%%%%%%%%%%%%
% Check that small diameter of taper will not yield
%%%%%%%%%%%%%%%%%%%%%%%%%%%%%%%%%%%%%%%%%%%%%%%%%%%%%%%%%%%%

c_d_a=r_tilt_taper_min;                 %distance to neutral axis [m]

circum_stress_d_a=-((r_tilt_taper_min^2+r_tilt_inner^2)*p)/...
    (r_tilt_taper_min^2-r_tilt_inner^2);    %circumfrential stress [Pa]
radial_stress_d_a=-p;                       %radial stress [Pa]
bend_stress_d_a=M_stress*c_d_a/I_x;         %bending stress [Pa]

if bend_stress_d_a>sigma_yield || circum_stress_d_a>sigma_yield ||...
        radial_stress_d_a>sigma_yield
    display('Tilt shaft will yield at small end of taper.')
```

```
266 else display('Tilt shaft will not yield at small end of taper.')
267 end
268
269
270 %%%%%%%%%%%%%%%%%%%%%%%%%%%%%%%%%%%%%%%%%%%%%%%%%%%%
271 % Check that open hub of flange will not yield
272 %%%%%%%%%%%%%%%%%%%%%%%%%%%%%%%%%%%%%%%%%%%%%%%%%%%%
273
274 %flange thickness at large end of taper [m]
275 t_flange_hub_min=r_flange_outer-r_tilt_taper_max;
276
277 %inner flange radius at larage diameter taper [m]
278 r_flange_inner_max=r_tilt_taper_max;
279 r_flange_outer_max=r_flange_outer;  %outer flange radius (constant) [m]
280
281 I_x_flange=(pi/64)*(r_flange_outer^4-r_flange_inner_max^4); %[m^4]
282 c_flange=r_flange_outer_max;        %distance to neutral axis [m]
283
284 %circumfrential stress [Pa]
285 circum_stress_r_flange_max=((r_flange_outer_max^2+r_flange_inner_max^2)*p)/...
286     (r_flange_outer_max^2-r_flange_inner_max^2);
287
288 radial_stress_r_flange_max=-p;  %radial stress [Pa]
289 bend_stress_r_flange_max=M_stress*c_flange/I_x_flange; %bending stress [Pa]
290
291 if bend_stress_r_flange_max>sigma_yield || circum_stress_r_flange_max...
292         >sigma_yield || radial_stress_r_flange_max>sigma_yield
293     display('Flange will yield at open end of hub.')
294 else display('Flange will not yield at open end of hub.')
295 end
296
```

```
297 %%%%%%%%%%%%%%%%%%%%%%%%%%%%%%%%%%%%%%%%%%%%%%%%%%%%%%%%
298 % Check that closed hub of flange will not yield
299 %%%%%%%%%%%%%%%%%%%%%%%%%%%%%%%%%%%%%%%%%%%%%%%%%%%%%%%%
300
301 %flange thickness at small end of taper [m]
302 t_flange_hub_max=r_flange_outer-r_tilt_taper_min;
303
304 %inner flange radius at larage diameter taper [m]
305 r_flange_inner_min=r_tilt_taper_min;
306
307 I_x_flange_min=(pi/64)*(r_flange_outer^4-r_flange_inner_min^4); %[m^4]
308
309 %circumfrential stress [Pa]
310 circum_stress_r_flange_min=((r_flange_outer_max^2+r_flange_inner_min^2)*p)/...
311     (r_flange_outer_max^2-r_flange_inner_min^2);
312
313 radial_stress_r_flange_min=-p;  %radial stress [Pa]
314
315 %bending stress [Pa]
316 bend_stress_r_flange_min=M_stress*c_flange/I_x_flange_min;
317
318 if bend_stress_r_flange_min>sigma_yield || circum_stress_r_flange_min...
319         >sigma_yield || radial_stress_r_flange_min>sigma_yield
320     display('Flange will yield at closed end of hub.')
321 else display('Flange will not yield at closed end of hub.')
322 end
323
324 %%%%%%%%%%%%%%%%
325 % End of Script
326 %%%%%%%%%%%%%%%%
```

THIS PAGE INTENTIONALLY LEFT BLANK

Appendix C

Shock Testing Analysis Mathematical Code

```
%%%%%%%%%%%%%%%%%%%%%%%%%%%%%%%%%%%%%%%%%%%%%%%%%%%%%%%%%%%%%%%%%%%%%%%%%%%%
% This script analyzes the shock rig confidence tests with damper
%%%%%%%%%%%%%%%%%%%%%%%%%%%%%%%%%%%%%%%%%%%%%%%%%%%%%%%%%%%%%%%%%%%%%%%%%%%%

clf
clear all
close all
clc


%%%%%%%%%%%%%%%%%%%%%%%%%%%%%%%%%%%%%%%%%%%%%%%%
% 10 Degrees
%%%%%%%%%%%%%%%%%%%%%%%%%%%%%%%%%%%%%%%%%%%%%%%%

% Create matrices for time and accelerometer
```

```
Test10 = csvread('10Degrees.csv',1,0);
Test10_time = Test10([1:end],[1]);
Test10_1 = Test10([1:end],[3]);
Test10_2 = Test10([1:end],[6]);
Test10_3 = Test10([1:end],[9]);
Test10_4 = Test10([1:end],[12]);
Test10_5 = Test10([1:end],[15]);

% Determine window size for moving average by plotting the sum of absolute
% differences for different window sizes and finding the knee in the curve,
% where the window is smallest and the curve seems to flatten. Maximum
% window size is calculated from a 10 kHz sample rate over the duration of
% the impulse.
windowSizes = 1 : 1 : 89;
for k = 1 : length(windowSizes);
    smoothed1 = movmean(Test10_1, windowSizes(k));
    sad1(k) = sum(abs(smoothed1 - Test10_1));
    smoothed2 = movmean(Test10_2, windowSizes(k));
    sad2(k) = sum(abs(smoothed2 - Test10_2));
    smoothed3 = movmean(Test10_3, windowSizes(k));
    sad3(k) = sum(abs(smoothed3 - Test10_3));
    smoothed4 = movmean(Test10_4, windowSizes(k));
    sad4(k) = sum(abs(smoothed4 - Test10_4));
    smoothed5 = movmean(Test10_5, windowSizes(k));
    sad5(k) = sum(abs(smoothed5 - Test10_5));
end

figure('Name','10 Degrees - SAD')
subplot(5,1,1);
plot(windowSizes, sad1, 'b*-', 'LineWidth', 2);
title('SAD 10-1')
```

```
47 grid on;
48 xlabel('Window Size');
49 ylabel('Sum of Absolute Differences');
50 subplot(5,1,2);
51 plot(windowSizes, sad2, 'b*-', 'LineWidth', 2);
52 title('SAD 10-2')
53 grid on;
54 xlabel('Window Size');
55 ylabel('Sum of Absolute Differences');
56 subplot(5,1,3);
57 plot(windowSizes, sad3, 'b*-', 'LineWidth', 2);
58 title('SAD 10-3')
59 grid on;
60 xlabel('Window Size');
61 ylabel('Sum of Absolute Differences');
62 subplot(5,1,4);
63 plot(windowSizes, sad4, 'b*-', 'LineWidth', 2);
64 title('SAD 10-4')
65 grid on;
66 xlabel('Window Size');
67 ylabel('Sum of Absolute Differences');
68 subplot(5,1,5);
69 plot(windowSizes, sad5, 'b*-', 'LineWidth', 2);
70 title('SAD 10-5')
71 grid on;
72 xlabel('Window Size');
73 ylabel('Sum of Absolute Differences');
74
75 % Moving Average Filter
76 Test10_1smooth = smoothdata(Test10_1,'movmean',44);
77 Test10_2smooth = smoothdata(Test10_2,'movmean',44);
```

```
78 Test10_3smooth = smoothdata(Test10_3,'movmean',44);
79 Test10_4smooth = smoothdata(Test10_4,'movmean',44);
80 Test10_5smooth = smoothdata(Test10_5,'movmean',44);
81
82 % Find maximum accelerations of each run, then average
83 Max10_1 = max(abs(max(Test10_1)),abs(min(Test10_1)));
84 Max10_1smooth = max(abs(max(Test10_1smooth)),abs(min(Test10_1smooth)));
85 Max10_2 = max(abs(max(Test10_2)),abs(min(Test10_2)));
86 Max10_2smooth = max(abs(max(Test10_2smooth)),abs(min(Test10_2smooth)));
87 Max10_3 = max(abs(max(Test10_3)),abs(min(Test10_3)));
88 Max10_3smooth = max(abs(max(Test10_3smooth)),abs(min(Test10_3smooth)));
89 Max10_4 = max(abs(max(Test10_4)),abs(min(Test10_4)));
90 Max10_4smooth = max(abs(max(Test10_4smooth)),abs(min(Test10_4smooth)));
91 Max10_5 = max(abs(max(Test10_5)),abs(min(Test10_5)));
92 Max10_5smooth = max(abs(max(Test10_5smooth)),abs(min(Test10_5smooth)));
93
94 M_10 = [Max10_1 Max10_2 Max10_3 Max10_4 Max10_5];
95 M_10 = mean(M_10);
96
97 G_1 = [Max10_1smooth; Max10_2smooth; Max10_3smooth; Max10_4smooth;...
98     Max10_5smooth];
99 G_10 = mean(G_1);
100
101 % Determine 95% confidence interval of data
102 pd10 = fitdist(G_1,'Normal');
103 ci10 = paramci(pd10);
104
105 % Plot raw and smooth data
106 figure('Name','10 Degrees')
107 plot(Test10_time,Test10_3,'-','LineWidth',1)
108 hold on
```

```
109 plot(Test10_time,Test10_3smooth,'-','LineWidth',1)
110 hold on
111 xlim([-0.01 0.09])
112
113 title('Acceleration v. Time for 10 Degrees at 10 kHz')
114 xlabel('Time [s]')
115 ylabel('Acceleration [G-forces]')
116 legend('Data','Smoothed Data')
117 str = {'Max Measured Acceleration =' M_10,...
118    'Mean Moving Average Acceleration =' G_10};
119 annotation('textbox',[.5 .7 .1 .1],'String',str,'FitBoxToText','on');
120
121
122 %%%%%%%%%%%%%%%%%%%%%%%%%%%%%%%%%%%%%%%%%%%%
123 % 20 Degrees
124 %%%%%%%%%%%%%%%%%%%%%%%%%%%%%%%%%%%%%%%%%%%%
125
126 % Create matrices for time and accelerometer
127 Test20 = csvread('20Degrees.csv',1,0);
128 Test20_time = Test10([1:end],[1]);
129 Test20_1 = Test20([1:end],[3]);
130 Test20_2 = Test20([1:end],[6]);
131 Test20_3 = Test20([1:end],[9]);
132 Test20_4 = Test20([1:end],[12]);
133 Test20_5 = Test20([1:end],[15]);
134
135 % Determine window size for moving average by plotting the sum of absolute
136 % differences for different window sizes and finding the knee in the curve,
137 % where the window is smallest and the curve seems to flatten. Maximum
138 % window size is calculated from a 10 kHz sample rate over the duration of
139 % the impulse.
```

```
windowSizes = 1 : 1 : 89;
for k = 1 : length(windowSizes);
    smoothed1 = movmean(Test20_1, windowSizes(k));
    sad1(k) = sum(abs(smoothed1 - Test20_1));
    smoothed2 = movmean(Test20_2, windowSizes(k));
    sad2(k) = sum(abs(smoothed2 - Test20_2));
    smoothed3 = movmean(Test20_3, windowSizes(k));
    sad3(k) = sum(abs(smoothed3 - Test20_3));
    smoothed4 = movmean(Test20_4, windowSizes(k));
    sad4(k) = sum(abs(smoothed4 - Test20_4));
    smoothed5 = movmean(Test20_5, windowSizes(k));
    sad5(k) = sum(abs(smoothed5 - Test20_5));
end

figure('Name','20 Degrees - SAD')
subplot(5,1,1);
plot(windowSizes, sad1, 'b*-', 'LineWidth', 2);
title('SAD 20-1')
grid on;
xlabel('Window Size');
ylabel('Sum of Absolute Differences');
subplot(5,1,2);
plot(windowSizes, sad2, 'b*-', 'LineWidth', 2);
title('SAD 20-2')
grid on;
xlabel('Window Size');
ylabel('Sum of Absolute Differences');
subplot(5,1,3);
plot(windowSizes, sad3, 'b*-', 'LineWidth', 2);
title('SAD 20-3')
grid on;
```

```
171 xlabel('Window Size');
172 ylabel('Sum of Absolute Differences');
173 subplot(5,1,4);
174 plot(windowSizes, sad4, 'b*-', 'LineWidth', 2);
175 title('SAD 20-4')
176 grid on;
177 xlabel('Window Size');
178 ylabel('Sum of Absolute Differences');
179 subplot(5,1,5);
180 plot(windowSizes, sad5, 'b*-', 'LineWidth', 2);
181 title('SAD 20-5')
182 grid on;
183 xlabel('Window Size');
184 ylabel('Sum of Absolute Differences');
185
186 % Moving Average Filter
187 Test20_1smooth = smoothdata(Test20_1,'movmean',44);
188 Test20_2smooth = smoothdata(Test20_2,'movmean',44);
189 Test20_3smooth = smoothdata(Test20_3,'movmean',44);
190 Test20_4smooth = smoothdata(Test20_4,'movmean',44);
191 Test20_5smooth = smoothdata(Test20_5,'movmean',44);
192
193 % Find maximum accelerations of each run, then average
194 Max20_1 = max(abs(max(Test20_1)),abs(min(Test20_1)));
195 Max20_1smooth = max(abs(max(Test20_1smooth)),abs(min(Test20_1smooth)));
196 Max20_2 = max(abs(max(Test20_2)),abs(min(Test20_2)));
197 Max20_2smooth = max(abs(max(Test20_2smooth)),abs(min(Test20_2smooth)));
198 Max20_3 = max(abs(max(Test20_3)),abs(min(Test20_3)));
199 Max20_3smooth = max(abs(max(Test20_3smooth)),abs(min(Test20_3smooth)));
200 Max20_4 = max(abs(max(Test20_4)),abs(min(Test20_4)));
201 Max20_4smooth = max(abs(max(Test20_4smooth)),abs(min(Test20_4smooth)));
```

```
202 Max20_5 = max(abs(max(Test20_5)),abs(min(Test20_5)));
203 Max20_5smooth = max(abs(max(Test20_5smooth)),abs(min(Test20_5smooth)));
204
205 M_20 = [Max20_1 Max20_2 Max20_3 Max20_4 Max20_5];
206 M_20 = mean(M_20);
207
208 G_2 = [Max20_1smooth; Max20_2smooth; Max20_3smooth; Max20_4smooth;...
209     Max20_5smooth];
210 G_20 = mean(G_2);
211
212 % Determine 95% confidence interval of data
213 pd20 = fitdist(G_2,'Normal');
214 ci20 = paramci(pd20);
215
216 % Plot raw and smooth data
217 figure('Name','20 Degrees')
218 plot(Test20_time,Test20_3,'-','LineWidth',1)
219 hold on
220 plot(Test20_time,Test20_3smooth,'-','LineWidth',1)
221 hold on
222 xlim([-0.01 0.09])
223
224 title('Acceleration v. Time for 20 Degrees at 10 kHz')
225 xlabel('Time [s]')
226 ylabel('Acceleration [G-forces]')
227 legend('Raw Data','Smoothed Data')
228 str = {'Max Measured Acceleration =' M_20,...
229    'Mean Moving Average Acceleration =' G_20};
230 annotation('textbox',[.5 .7 .1 .1],'String',str,'FitBoxToText','on');
231
232
```

```
%%%%%%%%%%%%%%%%%%%%%%%%%%%%%%%%%%%%%%%%%%%%
% 30 Degrees
%%%%%%%%%%%%%%%%%%%%%%%%%%%%%%%%%%%%%%%%%%%%

% Create matrices for time and accelerometer
Test30 = csvread('30Degrees.csv',1,0);
Test30_time = Test30([1:end],[1]);
Test30_1 = Test30([1:end],[3]);
Test30_2 = Test30([1:end],[6]);
Test30_3 = Test30([1:end],[9]);
Test30_4 = Test30([1:end],[12]);
Test30_5 = Test30([1:end],[15]);

% Determine window size for moving average by plotting the sum of absolute
% differences for different window sizes and finding the knee in the curve,
% where the window is smallest and the curve seems to flatten. Maximum
% window size is calculated from a 10 kHz sample rate over the duration of
% the impulse.
windowSizes = 1 : 1 : 89;
for k = 1 : length(windowSizes);
    smoothed1 = movmean(Test30_1, windowSizes(k));
    sad1(k) = sum(abs(smoothed1 - Test30_1));
    smoothed2 = movmean(Test30_2, windowSizes(k));
    sad2(k) = sum(abs(smoothed2 - Test30_2));
    smoothed3 = movmean(Test30_3, windowSizes(k));
    sad3(k) = sum(abs(smoothed3 - Test30_3));
    smoothed4 = movmean(Test30_4, windowSizes(k));
    sad4(k) = sum(abs(smoothed4 - Test30_4));
    smoothed5 = movmean(Test30_5, windowSizes(k));
    sad5(k) = sum(abs(smoothed5 - Test30_5));
end
```

```
264
265 figure('Name','30 Degrees - SAD')
266 subplot(5,1,1);
267 plot(windowSizes, sad1, 'b*-', 'LineWidth', 2);
268 title('SAD 30-1')
269 grid on;
270 xlabel('Window Size');
271 ylabel('Sum of Absolute Differences');
272 subplot(5,1,2);
273 plot(windowSizes, sad2, 'b*-', 'LineWidth', 2);
274 title('SAD 30-2')
275 grid on;
276 xlabel('Window Size');
277 ylabel('Sum of Absolute Differences');
278 subplot(5,1,3);
279 plot(windowSizes, sad3, 'b*-', 'LineWidth', 2);
280 title('SAD 30-3')
281 grid on;
282 xlabel('Window Size');
283 ylabel('Sum of Absolute Differences');
284 subplot(5,1,4);
285 plot(windowSizes, sad4, 'b*-', 'LineWidth', 2);
286 title('SAD 30-4')
287 grid on;
288 xlabel('Window Size');
289 ylabel('Sum of Absolute Differences');
290 subplot(5,1,5);
291 plot(windowSizes, sad5, 'b*-', 'LineWidth', 2);
292 title('SAD 30-5')
293 grid on;
294 xlabel('Window Size');
```

```
ylabel('Sum of Absolute Differences');

% Moving Average Filter
Test30_1smooth = smoothdata(Test30_1,'movmean',52);
Test30_2smooth = smoothdata(Test30_2,'movmean',52);
Test30_3smooth = smoothdata(Test30_3,'movmean',52);
Test30_4smooth = smoothdata(Test30_4,'movmean',52);
Test30_5smooth = smoothdata(Test30_5,'movmean',52);

% Find maximum accelerations of each run, then average
Max30_1 = max(abs(max(Test30_1)),abs(min(Test30_1)));
Max30_1smooth = max(abs(max(Test30_1smooth)),abs(min(Test30_1smooth)));
Max30_2 = max(abs(max(Test30_2)),abs(min(Test30_2)));
Max30_2smooth = max(abs(max(Test30_2smooth)),abs(min(Test30_2smooth)));
Max30_3 = max(abs(max(Test30_3)),abs(min(Test30_3)));
Max30_3smooth = max(abs(max(Test30_3smooth)),abs(min(Test30_3smooth)));
Max30_4 = max(abs(max(Test30_4)),abs(min(Test30_4)));
Max30_4smooth = max(abs(max(Test30_4smooth)),abs(min(Test30_4smooth)));
Max30_5 = max(abs(max(Test30_5)),abs(min(Test30_5)));
Max30_5smooth = max(abs(max(Test30_5smooth)),abs(min(Test30_5smooth)));

M_30 = [Max30_1 Max30_2 Max30_3 Max30_4 Max30_5];
M_30 = mean(M_30);

G_3 = [Max30_1smooth; Max30_2smooth; Max30_3smooth; Max30_4smooth;...
    Max30_5smooth];
G_30 = mean(G_3);

% Determine 95% confidence interval of data
pd30 = fitdist(G_3,'Normal');
ci30 = paramci(pd30);
```

```
326
327 % Plot raw and smooth data
328 figure('Name','30 Degrees')
329 plot(Test30_time,Test30_3,'-','LineWidth',1)
330 hold on
331 plot(Test30_time,Test30_3smooth,'-','LineWidth',1)
332 hold on
333 xlim([-0.01 0.09])
334
335 title('Acceleration v. Time for 30 Degrees at 10 kHz')
336 xlabel('Time [s]')
337 ylabel('Acceleration [G-forces]')
338 legend('Raw Data','Smoothed Data')
339 str = {'Max Measured Acceleration =' M_30,...
340    'Mean Moving Average Acceleration =' G_30};
341 annotation('textbox',[.5 .7 .1 .1],'String',str,'FitBoxToText','on');
342
343
344 %%%%%%%%%%%%%%%%%%%%%%%%%%%%%%%%%%%%%%%%%%%%
345 % 40 Degrees
346 %%%%%%%%%%%%%%%%%%%%%%%%%%%%%%%%%%%%%%%%%%%%
347
348 % Create matrices for time and accelerometer
349 Test40 = csvread('40Degrees.csv',1,0);
350 Test40_time = Test40([1:end],[1]);
351 Test40_1 = Test40([1:end],[3]);
352 Test40_2 = Test40([1:end],[6]);
353 Test40_3 = Test40([1:end],[9]);
354 Test40_4 = Test40([1:end],[12]);
355 Test40_5 = Test40([1:end],[15]);
356
```

```
% Determine window size for moving average by plotting the sum of absolute
% differences for different window sizes and finding the knee in the curve,
% where the window is smallest and the curve seems to flatten. Maximum
% window size is calculated from a 10 kHz sample rate over the duration of
% the impulse.
windowSizes = 1 : 1 : 89;
for k = 1 : length(windowSizes);
    smoothed1 = movmean(Test40_1, windowSizes(k));
    sad1(k) = sum(abs(smoothed1 - Test40_1));
    smoothed2 = movmean(Test40_2, windowSizes(k));
    sad2(k) = sum(abs(smoothed2 - Test40_2));
    smoothed3 = movmean(Test40_3, windowSizes(k));
    sad3(k) = sum(abs(smoothed3 - Test40_3));
    smoothed4 = movmean(Test40_4, windowSizes(k));
    sad4(k) = sum(abs(smoothed4 - Test40_4));
    smoothed5 = movmean(Test40_5, windowSizes(k));
    sad5(k) = sum(abs(smoothed5 - Test40_5));
end

figure('Name','40 Degrees - SAD')
subplot(5,1,1);
plot(windowSizes, sad1, 'b*-', 'LineWidth', 2);
title('SAD 40-1')
grid on;
xlabel('Window Size');
ylabel('Sum of Absolute Differences');
subplot(5,1,2);
plot(windowSizes, sad2, 'b*-', 'LineWidth', 2);
title('SAD 40-2')
grid on;
xlabel('Window Size');
```

```
388 ylabel('Sum of Absolute Differences');
389 subplot(5,1,3);
390 plot(windowSizes, sad3, 'b*-', 'LineWidth', 2);
391 title('SAD 40-3')
392 grid on;
393 xlabel('Window Size');
394 ylabel('Sum of Absolute Differences');
395 subplot(5,1,4);
396 plot(windowSizes, sad4, 'b*-', 'LineWidth', 2);
397 title('SAD 40-4')
398 grid on;
399 xlabel('Window Size');
400 ylabel('Sum of Absolute Differences');
401 subplot(5,1,5);
402 plot(windowSizes, sad5, 'b*-', 'LineWidth', 2);
403 title('SAD 40-5')
404 grid on;
405 xlabel('Window Size');
406 ylabel('Sum of Absolute Differences');
407
408 % Moving Average Filter
409 Test40_1smooth = smoothdata(Test40_1,'movmean',52);
410 Test40_2smooth = smoothdata(Test40_2,'movmean',52);
411 Test40_3smooth = smoothdata(Test40_3,'movmean',52);
412 Test40_4smooth = smoothdata(Test40_4,'movmean',52);
413 Test40_5smooth = smoothdata(Test40_5,'movmean',52);
414
415 % Find maximum accelerations of each run, then average
416 Max40_1 = max(abs(max(Test40_1)),abs(min(Test40_1)));
417 Max40_1smooth = max(abs(max(Test40_1smooth)),abs(min(Test40_1smooth)));
418 Max40_2 = max(abs(max(Test40_2)),abs(min(Test40_2)));
```

```
Max40_2smooth = max(abs(max(Test40_2smooth)),abs(min(Test40_2smooth)));
Max40_3 = max(abs(max(Test40_3)),abs(min(Test40_3)));
Max40_3smooth = max(abs(max(Test40_3smooth)),abs(min(Test40_3smooth)));
Max40_4 = max(abs(max(Test40_4)),abs(min(Test40_4)));
Max40_4smooth = max(abs(max(Test40_4smooth)),abs(min(Test40_4smooth)));
Max40_5 = max(abs(max(Test40_5)),abs(min(Test40_5)));
Max40_5smooth = max(abs(max(Test40_5smooth)),abs(min(Test40_5smooth)));

M_40 = [Max40_1 Max40_2 Max40_3 Max40_4 Max40_5];
M_40 = mean(M_40);

G_4 = [Max40_1smooth; Max40_2smooth; Max40_3smooth; Max40_4smooth;...
    Max40_5smooth];
G_40 = mean(G_4);

% Determine 95% confidence interval of data
pd40 = fitdist(G_4,'Normal');
ci40 = paramci(pd40);

% Plot raw and smooth data
figure('Name','40 Degrees')
plot(Test40_time,Test40_3,'-','LineWidth',1)
hold on
plot(Test40_time,Test40_3smooth,'-','LineWidth',1)
hold on
xlim([-0.01 0.09])

title('Acceleration v. Time for 40 Degrees at 10 kHz')
xlabel('Time [s]')
ylabel('Acceleration [G-forces]')
legend('Raw Data','Smoothed Data')
```

```
str = {'Max Measured Acceleration =' M_40,...
    'Mean Moving Average Acceleration =' G_40};
annotation('textbox',[.5 .7 .1 .1],'String',str,'FitBoxToText','on');


%%%%%%%%%%%%%%%%%%%%%%%%%%%%%%%%%%%%%%%%%%%%
% 50 Degrees
%%%%%%%%%%%%%%%%%%%%%%%%%%%%%%%%%%%%%%%%%%%%

% Create matrices for time and accelerometer
Test50 = csvread('50Degrees.csv',1,0);
Test50_time = Test50([1:end],[1]);
Test50_1 = Test50([1:end],[3]);
Test50_2 = Test50([1:end],[6]);
Test50_3 = Test50([1:end],[9]);
Test50_4 = Test50([1:end],[12]);
Test50_5 = Test50([1:end],[15]);

% Determine window size for moving average by plotting the sum of absolute
% differences for different window sizes and finding the knee in the curve,
% where the window is smallest and the curve seems to flatten. Maximum
% window size is calculated from a 10 kHz sample rate over the duration of
% the impulse.
windowSizes = 1 : 1 : 89;
for k = 1 : length(windowSizes);
    smoothed1 = movmean(Test50_1, windowSizes(k));
    sad1(k) = sum(abs(smoothed1 - Test50_1));
    smoothed2 = movmean(Test50_2, windowSizes(k));
    sad2(k) = sum(abs(smoothed2 - Test50_2));
    smoothed3 = movmean(Test50_3, windowSizes(k));
    sad3(k) = sum(abs(smoothed3 - Test50_3));
```

```
481     smoothed4 = movmean(Test50_4, windowSizes(k));
482     sad4(k) = sum(abs(smoothed4 - Test50_4));
483     smoothed5 = movmean(Test50_5, windowSizes(k));
484     sad5(k) = sum(abs(smoothed5 - Test50_5));
485 end
486
487 figure('Name','50 Degrees - SAD')
488 subplot(5,1,1);
489 plot(windowSizes, sad1, 'b*-', 'LineWidth', 2);
490 title('SAD 50-1')
491 grid on;
492 xlabel('Window Size');
493 ylabel('Sum of Absolute Differences');
494 subplot(5,1,2);
495 plot(windowSizes, sad2, 'b*-', 'LineWidth', 2);
496 title('SAD 50-2')
497 grid on;
498 xlabel('Window Size');
499 ylabel('Sum of Absolute Differences');
500 subplot(5,1,3);
501 plot(windowSizes, sad3, 'b*-', 'LineWidth', 2);
502 title('SAD 50-3')
503 grid on;
504 xlabel('Window Size');
505 ylabel('Sum of Absolute Differences');
506 subplot(5,1,4);
507 plot(windowSizes, sad4, 'b*-', 'LineWidth', 2);
508 title('SAD 50-4')
509 grid on;
510 xlabel('Window Size');
511 ylabel('Sum of Absolute Differences');
```

```
512 subplot(5,1,5);
513 plot(windowSizes, sad5, 'b*-', 'LineWidth', 2);
514 title('SAD 50-5')
515 grid on;
516 xlabel('Window Size');
517 ylabel('Sum of Absolute Differences');
518
519 % Moving Average Filter
520 Test50_1smooth = smoothdata(Test50_1,'movmean',52);
521 Test50_2smooth = smoothdata(Test50_2,'movmean',52);
522 Test50_3smooth = smoothdata(Test50_3,'movmean',52);
523 Test50_4smooth = smoothdata(Test50_4,'movmean',52);
524 Test50_5smooth = smoothdata(Test50_5,'movmean',52);
525
526 % Find maximum accelerations of each run, then average
527 Max50_1 = max(abs(max(Test50_1)),abs(min(Test50_1)));
528 Max50_1smooth = max(abs(max(Test50_1smooth)),abs(min(Test50_1smooth)));
529 Max50_2 = max(abs(max(Test50_2)),abs(min(Test50_2)));
530 Max50_2smooth = max(abs(max(Test50_2smooth)),abs(min(Test50_2smooth)));
531 Max50_3 = max(abs(max(Test50_3)),abs(min(Test50_3)));
532 Max50_3smooth = max(abs(max(Test50_3smooth)),abs(min(Test50_3smooth)));
533 Max50_4 = max(abs(max(Test50_4)),abs(min(Test50_4)));
534 Max50_4smooth = max(abs(max(Test50_4smooth)),abs(min(Test50_4smooth)));
535 Max50_5 = max(abs(max(Test50_5)),abs(min(Test50_5)));
536 Max50_5smooth = max(abs(max(Test50_5smooth)),abs(min(Test50_5smooth)));
537
538 M_50 = [Max50_1 Max50_2 Max50_3 Max50_4 Max50_5];
539 M_50 = mean(M_50);
540
541 G_5 = [Max50_1smooth; Max50_2smooth; Max50_3smooth; Max50_4smooth;...
542     Max50_5smooth];
```

```
543 G_50 = mean(G_5);
544
545 % Determine 95% confidence interval of data
546 pd50 = fitdist(G_5,'Normal');
547 ci50 = paramci(pd50);
548
549 % Plot raw and smooth data
550 figure('Name','50 Degrees')
551 plot(Test50_time,Test50_3,'-','LineWidth',1)
552 hold on
553 plot(Test50_time,Test50_3smooth,'-','LineWidth',1)
554 hold on
555 xlim([-0.01 0.09])
556
557 title('Acceleration v. Time for 50 Degrees at 10 kHz')
558 xlabel('Time [s]')
559 ylabel('Acceleration [G-forces]')
560 legend('Raw Data','Smoothed Data')
561 str = {'Max Measured Acceleration =' M_50,...
562    'Mean Moving Average Acceleration =' G_50};
563 annotation('textbox',[.5 .7 .1 .1],'String',str,'FitBoxToText','on');
564
565
566 %%%%%%%%%%%%%%%%%%%%%%%%%%%%%%%%%%%%%%%%%%%%
567 % 60 Degrees
568 %%%%%%%%%%%%%%%%%%%%%%%%%%%%%%%%%%%%%%%%%%%%
569
570 % Create matrices for time and accelerometer
571 Test60 = csvread('60Degrees.csv',1,0);
572 Test60_time = Test60([1:end],[1]);
573 Test60_1 = Test60([1:end],[3]);
```

```
574 Test60_2 = Test60([1:end],[6]);
575 Test60_3 = Test60([1:end],[9]);
576 Test60_4 = Test60([1:end],[12]);
577 Test60_5 = Test60([1:end],[15]);
578
579 % Determine window size for moving average by plotting the sum of absolute
580 % differences for different window sizes and finding the knee in the curve,
581 % where the window is smallest and the curve seems to flatten. Maximum
582 % window size is calculated from a 10 kHz sample rate over the duration of
583 % the impulse.
584 windowSizes = 1 : 1 : 89;
585 for k = 1 : length(windowSizes);
586     smoothed1 = movmean(Test60_1, windowSizes(k));
587     sad1(k) = sum(abs(smoothed1 - Test60_1));
588     smoothed2 = movmean(Test60_2, windowSizes(k));
589     sad2(k) = sum(abs(smoothed2 - Test60_2));
590     smoothed3 = movmean(Test60_3, windowSizes(k));
591     sad3(k) = sum(abs(smoothed3 - Test60_3));
592     smoothed4 = movmean(Test60_4, windowSizes(k));
593     sad4(k) = sum(abs(smoothed4 - Test60_4));
594     smoothed5 = movmean(Test60_5, windowSizes(k));
595     sad5(k) = sum(abs(smoothed5 - Test60_5));
596 end
597
598 figure('Name','60 Degrees - SAD')
599 subplot(5,1,1);
600 plot(windowSizes, sad1, 'b*-', 'LineWidth', 2);
601 title('SAD 60-1')
602 grid on;
603 xlabel('Window Size');
604 ylabel('Sum of Absolute Differences');
```

```
605 subplot(5,1,2);
606 plot(windowSizes, sad2, 'b*-', 'LineWidth', 2);
607 title('SAD 60-2')
608 grid on;
609 xlabel('Window Size');
610 ylabel('Sum of Absolute Differences');
611 subplot(5,1,3);
612 plot(windowSizes, sad3, 'b*-', 'LineWidth', 2);
613 title('SAD 60-3')
614 grid on;
615 xlabel('Window Size');
616 ylabel('Sum of Absolute Differences');
617 subplot(5,1,4);
618 plot(windowSizes, sad4, 'b*-', 'LineWidth', 2);
619 title('SAD 60-4')
620 grid on;
621 xlabel('Window Size');
622 ylabel('Sum of Absolute Differences');
623 subplot(5,1,5);
624 plot(windowSizes, sad5, 'b*-', 'LineWidth', 2);
625 title('SAD 60-5')
626 grid on;
627 xlabel('Window Size');
628 ylabel('Sum of Absolute Differences');
629
630 % Moving Average Filter
631 Test60_1smooth = smoothdata(Test60_1,'movmean',52);
632 Test60_2smooth = smoothdata(Test60_2,'movmean',52);
633 Test60_3smooth = smoothdata(Test60_3,'movmean',52);
634 Test60_4smooth = smoothdata(Test60_4,'movmean',52);
635 Test60_5smooth = smoothdata(Test60_5,'movmean',52);
```

```
636
637 % Find maximum accelerations of each run, then average
638 Max60_1 = max(abs(max(Test60_1)),abs(min(Test60_1)));
639 Max60_1smooth = max(abs(max(Test60_1smooth)),abs(min(Test60_1smooth)));
640 Max60_2 = max(abs(max(Test60_2)),abs(min(Test60_2)));
641 Max60_2smooth = max(abs(max(Test60_2smooth)),abs(min(Test60_2smooth)));
642 Max60_3 = max(abs(max(Test60_3)),abs(min(Test60_3)));
643 Max60_3smooth = max(abs(max(Test60_3smooth)),abs(min(Test60_3smooth)));
644 Max60_4 = max(abs(max(Test60_4)),abs(min(Test60_4)));
645 Max60_4smooth = max(abs(max(Test60_4smooth)),abs(min(Test60_4smooth)));
646 Max60_5 = max(abs(max(Test60_5)),abs(min(Test60_5)));
647 Max60_5smooth = max(abs(max(Test60_5smooth)),abs(min(Test60_5smooth)));
648
649 M_60 = [Max60_1 Max60_2 Max60_3 Max60_4 Max60_5];
650 M_60 = mean(M_60);
651
652 G_6 = [Max60_1smooth; Max60_2smooth; Max60_3smooth; Max60_4smooth;...
653     Max60_5smooth];
654 G_60 = mean(G_6);
655
656 % Determine 95% confidence interval of data
657 pd60 = fitdist(G_6,'Normal');
658 ci60 = paramci(pd60);
659
660 % Plot raw and smooth data
661 figure('Name','60 Degrees')
662 plot(Test60_time,Test60_3,'-','LineWidth',1)
663 hold on
664 plot(Test60_time,Test60_3smooth,'-','LineWidth',1)
665 hold on
666 xlim([-0.01 0.09])
```

```
667
668 title('Acceleration v. Time for 60 Degrees at 10 kHz')
669 xlabel('Time [s]')
670 ylabel('Acceleration [G-forces]')
671 legend('Raw Data','Smoothed Data')
672 str = {'Max Measured Acceleration =' M_60,...
673    'Mean Moving Average Acceleration =' G_60};
674 annotation('textbox',[.5 .7 .1 .1],'String',str,'FitBoxToText','on');
675
676
677 %%%%%%%%%%%%%%%%%%%%%%%%%%%%%%%%%%%%%%%%%%%%
678 % 70 Degrees
679 %%%%%%%%%%%%%%%%%%%%%%%%%%%%%%%%%%%%%%%%%%%%
680
681 % Create matrices for time and accelerometer
682 Test70 = csvread('70Degrees.csv',1,0);
683 Test70_time = Test70([1:end],[1]);
684 Test70_1 = Test70([1:end],[3]);
685 Test70_2 = Test70([1:end],[6]);
686 Test70_3 = Test70([1:end],[9]);
687 Test70_4 = Test70([1:end],[12]);
688 Test70_5 = Test70([1:end],[15]);
689
690 % Determine window size for moving average by plotting the sum of absolute
691 % differences for different window sizes and finding the knee in the curve,
692 % where the window is smallest and the curve seems to flatten. Maximum
693 % window size is calculated from a 10 kHz sample rate over the duration of
694 % the impulse.
695 windowSizes = 1 : 1 : 89;
696 for k = 1 : length(windowSizes);
697     smoothed1 = movmean(Test70_1, windowSizes(k));
```

```
698     sad1(k) = sum(abs(smoothed1 - Test70_1));
699     smoothed2 = movmean(Test70_2, windowSizes(k));
700     sad2(k) = sum(abs(smoothed2 - Test70_2));
701     smoothed3 = movmean(Test70_3, windowSizes(k));
702     sad3(k) = sum(abs(smoothed3 - Test70_3));
703     smoothed4 = movmean(Test70_4, windowSizes(k));
704     sad4(k) = sum(abs(smoothed4 - Test70_4));
705     smoothed5 = movmean(Test70_5, windowSizes(k));
706     sad5(k) = sum(abs(smoothed5 - Test70_5));
707 end
708
709 figure('Name','70 Degrees - SAD')
710 subplot(5,1,1);
711 plot(windowSizes, sad1, 'b*-', 'LineWidth', 2);
712 title('SAD 70-1')
713 grid on;
714 xlabel('Window Size');
715 ylabel('Sum of Absolute Differences');
716 subplot(5,1,2);
717 plot(windowSizes, sad2, 'b*-', 'LineWidth', 2);
718 title('SAD 70-2')
719 grid on;
720 xlabel('Window Size');
721 ylabel('Sum of Absolute Differences');
722 subplot(5,1,3);
723 plot(windowSizes, sad3, 'b*-', 'LineWidth', 2);
724 title('SAD 70-3')
725 grid on;
726 xlabel('Window Size');
727 ylabel('Sum of Absolute Differences');
728 subplot(5,1,4);
```

```
729 plot(windowSizes, sad4, 'b*-', 'LineWidth', 2);
730 title('SAD 70-4')
731 grid on;
732 xlabel('Window Size');
733 ylabel('Sum of Absolute Differences');
734 subplot(5,1,5);
735 plot(windowSizes, sad5, 'b*-', 'LineWidth', 2);
736 title('SAD 70-5')
737 grid on;
738 xlabel('Window Size');
739 ylabel('Sum of Absolute Differences');
740
741 % Moving Average Filter
742 Test70_1smooth = smoothdata(Test70_1,'movmean',52);
743 Test70_2smooth = smoothdata(Test70_2,'movmean',52);
744 Test70_3smooth = smoothdata(Test70_3,'movmean',52);
745 Test70_4smooth = smoothdata(Test70_4,'movmean',52);
746 Test70_5smooth = smoothdata(Test70_5,'movmean',52);
747
748 % Find maximum accelerations of each run, then average
749 Max70_1 = max(abs(max(Test70_1)),abs(min(Test70_1)));
750 Max70_1smooth = max(abs(max(Test70_1smooth)),abs(min(Test70_1smooth)));
751 Max70_2 = max(abs(max(Test70_2)),abs(min(Test70_2)));
752 Max70_2smooth = max(abs(max(Test70_2smooth)),abs(min(Test70_2smooth)));
753 Max70_3 = max(abs(max(Test70_3)),abs(min(Test70_3)));
754 Max70_3smooth = max(abs(max(Test70_3smooth)),abs(min(Test70_3smooth)));
755 Max70_4 = max(abs(max(Test70_4)),abs(min(Test70_4)));
756 Max70_4smooth = max(abs(max(Test70_4smooth)),abs(min(Test70_4smooth)));
757 Max70_5 = max(abs(max(Test70_5)),abs(min(Test70_5)));
758 Max70_5smooth = max(abs(max(Test70_5smooth)),abs(min(Test70_5smooth)));
759
```

```
760 M_70 = [Max70_1 Max70_2 Max70_3 Max70_4 Max70_5];
761 M_70 = mean(M_70);
762
763 G_7 = [Max70_1smooth; Max70_2smooth; Max70_3smooth; Max70_4smooth;...
764     Max70_5smooth];
765 G_70 = mean(G_7);
766
767 % Determine 95% confidence interval of data
768 pd70 = fitdist(G_7,'Normal');
769 ci70 = paramci(pd70);
770
771 % Plot raw and smooth data
772 figure('Name','70 Degrees')
773 plot(Test70_time,Test70_3,'-','LineWidth',1)
774 hold on
775 plot(Test70_time,Test70_3smooth,'-','LineWidth',1)
776 hold on
777 xlim([-0.01 0.09])
778
779 title('Acceleration v. Time for 70 Degrees at 10 kHz')
780 xlabel('Time [s]')
781 ylabel('Acceleration [G-forces]')
782 legend('Raw Data','Smoothed Data')
783 str = {'Max Measured Acceleration =' M_70,...
784    'Mean Moving Average Acceleration =' G_70};
785 annotation('textbox',[.5 .7 .1 .1],'String',str,'FitBoxToText','on');
786
787
788 % Plot the acceleration versus angle
789
790 Angle = [10; 20; 30; 40; 50; 60; 70];
```

```
791 Acc = [G_10; G_20; G_30; G_40; G_50; G_60; G_70];
792 myfit = fit(Angle,Acc,'poly2');
793
794 figure('Name','Acceleration v. Angle')
795 plot(Angle,Acc,'+')
796 hold on
797 plot(myfit)
798 hold on
799 title('Acceleration v. Time for 70 Degrees at 10 kHz')
800 xlabel('Angle [deg]')
801 ylabel('Acceleration [G-forces]')
802 legend('Location','northwest','Mean Maximum Accelerations')
```

THIS PAGE INTENTIONALLY LEFT BLANK

Appendix D

Full Scale Testing Analysis Mathematical Code

```
%%%%%%%%%%%%%%%%%%%%%%%%%%%%%%%%%%%%%%%%%%%%%%%%%%%%%%%%%%%%%%%%%%%%%%%%
% This script plots the results of the full scale drop test
%%%%%%%%%%%%%%%%%%%%%%%%%%%%%%%%%%%%%%%%%%%%%%%%%%%%%%%%%%%%%%%%%%%%%%%%

clf
clear all
close all
clc


%%%%%%%%%%%%%%%%%%%%%%%%%%%%%%%%%%%%%%%%%%%%%%%%%%%%%%%%%%%%%%%%%%%%%%%%
% Run 1 Results with 70G and 500G Sensors
%%%%%%%%%%%%%%%%%%%%%%%%%%%%%%%%%%%%%%%%%%%%%%%%%%%%%%%%%%%%%%%%%%%%%%%%

% Create matrices for time, 70G data, and 500G data
```

```
Run1 = csvread('Run1.csv',1,0);
Run1_time = Run1([1:end],[1]);
Run1_time = Run1_time - Run1_time(1,1);
Run1_70 = Run1([1:end],[2]);
Run1_500 = Run1([1:end],[3]);

% Determine window size for moving average by plotting the sum of absolute
% differences for different window sizes and finding the knee in the curve,
% where the window is smallest and the curve seems to flatten. Maximum
% window size is calculated from a 10 kHz sample rate over the duration of
% the impulse.
windowSizes = 1 : 1 : 26;
for k = 1 : length(windowSizes);
    smoothed70 = movmean(Run1_70, windowSizes(k));
    sad70(k) = sum(abs(smoothed70 - Run1_70));
    smoothed500 = movmean(Run1_500, windowSizes(k));
    sad500(k) = sum(abs(smoothed500 - Run1_500));
end

figure('Name','Run 1 - SAD')
%subplot(2,1,1);
%plot(windowSizes, sad70, 'b*-', 'LineWidth', 2);
%title('SAD Run 1 70G')
%grid on;
%xlabel('Window Size');
%ylabel('Sum of Absolute Differences');
%subplot(2,1,2);
plot(windowSizes, sad500, 'b*-', 'LineWidth', 2);
title('SAD Run 1 500G')
grid on;
xlabel('Window Size');
```

```
47 ylabel('Sum of Absolute Differences');
48
49 % Moving Average Filter
50 Run1_70smooth = smoothdata(Run1_70,'movmean',4);
51 Run1_500smooth = smoothdata(Run1_500,'movmean',7);
52
53 % Find maximum accelerations captured by each sensor
54 Max_70_1 = max(abs(max(Run1_70)),abs(min(Run1_70)));
55 Max_500_1 = max(abs(max(Run1_500)),abs(min(Run1_500)));
56 Max_70_1_smooth = max(abs(max(Run1_70smooth)),abs(min(Run1_70smooth)));
57 Max_500_1_smooth = max(abs(max(Run1_500smooth)),abs(min(Run1_500smooth)));
58
59 % Plot raw and smooth data on single figure each
60 % figure('Name','Run 1 - 70G Sensor')
61 % plot(Run1_time,Run1_70,'-o','LineWidth',1,'color','k')
62 % hold on
63 % plot(Run1_time,Run1_70smooth,'-d','LineWidth',1,'color','r')
64 % hold on
65 %
66 % title('Acceleration v. Time for Full Scale Drop Test from 0.04445 m')
67 % xlabel('Time [s]')
68 % ylabel('Acceleration [G-forces]')
69 % legend('70G Sensor Data','70G Moving Average')
70 % str = {'Max Measured Acceleration 70G=' Max_70_1,...
71 %     'Max Moving Average Acceleration 70G=' Max_70_1_smooth};
72 % annotation('textbox',[.2 .75 .1 .1],'String',str,'FitBoxToText','on');
73
74 figure('Name','Run 1 - 500G')
75 plot(Run1_time,Run1_500,'-o','LineWidth',1,'color','k')
76 hold on
77 plot(Run1_time,Run1_500smooth,'-d','LineWidth',1,'color','r')
```

```
78 hold on
79
80 title('Acceleration v. Time for Full Scale Drop Test from 0.04445 m')
81 xlabel('Time [s]')
82 ylabel('Acceleration [G-forces]')
83 legend('500G Sensor Data','500G Moving Average')
84 str = {'Max Measured Acceleration 500G=' Max_500_1,...
85     'Max Moving Average Acceleration 500G=' Max_500_1_smooth};
86 annotation('textbox',[.2 .75 .1 .1],'String',str,'FitBoxToText','on');
87
88
89 %%%%%%%%%%%%%%%%%%%%%%%%%%%%%%%%%%%%%%%%%%%%
90 % Run 2 Results with 70G and 500G Sensors
91 %%%%%%%%%%%%%%%%%%%%%%%%%%%%%%%%%%%%%%%%%%%%
92
93 % Create matrices for time, 70G data, and 500G data
94 Run2 = csvread('Run2.csv',1,0);
95 Run2_time = Run2([1:end],[1]);
96 Run2_time = Run2_time - Run2_time(1,1);
97 Run2_70 = Run2([1:end],[2]);
98 Run2_500 = Run2([1:end],[3]);
99
100 % Determine window size for moving average by plotting the sum of absolute
101 % differences for different window sizes and finding the knee in the curve,
102 % where the window is smallest and the curve seems to flatten. Maximum
103 % window size is calculated from a 10 kHz sample rate over the duration of
104 % the impulse.
105 windowSizes = 1 : 1 : 26;
106 for k = 1 : length(windowSizes);
107     smoothed70 = movmean(Run2_70, windowSizes(k));
108     sad70(k) = sum(abs(smoothed70 - Run2_70));
```

```
109     smoothed500 = movmean(Run2_500, windowSizes(k));
110     sad500(k) = sum(abs(smoothed500 - Run2_500));
111 end
112
113 figure('Name','Run 2 - SAD')
114 % subplot(2,1,1);
115 % plot(windowSizes, sad70, 'b*-', 'LineWidth', 2);
116 % title('SAD Run 2 70G')
117 % grid on;
118 % xlabel('Window Size');
119 % ylabel('Sum of Absolute Differences');
120 % subplot(2,1,2);
121 plot(windowSizes, sad500, 'b*-', 'LineWidth', 2);
122 title('SAD Run 2 500G')
123 grid on;
124 xlabel('Window Size');
125 ylabel('Sum of Absolute Differences');
126
127 % Moving Average Filter
128 Run2_70smooth = smoothdata(Run2_70,'movmean',4);
129 Run2_500smooth = smoothdata(Run2_500,'movmean',7);
130
131 % Find maximum accelerations captured by each sensor
132 Max_70_2 = max(abs(max(Run2_70)),abs(min(Run2_70)));
133 Max_500_2 = max(abs(max(Run2_500)),abs(min(Run2_500)));
134 Max_70_2_smooth = max(abs(max(Run2_70smooth)),abs(min(Run2_70smooth)));
135 Max_500_2_smooth = max(abs(max(Run2_500smooth)),abs(min(Run2_500smooth)));
136
137 % Plot raw and smooth data on single figure each
138 % figure('Name','Run 2 - 70G')
139 % plot(Run2_time,Run2_70,'-o','LineWidth',1,'color','k')
```

```
% hold on
% plot(Run2_time,Run2_70smooth,'-d','LineWidth',1,'color','r')
% hold on
%
% title('Acceleration v. Time for Full Scale Drop Test from 0.2 m')
% xlabel('Time [s]')
% ylabel('Acceleration [G-forces]')
% legend('70G Sensor Data','70G Moving Average')
% str = {'Max Measured Acceleration 70G=' Max_70_2,...
%     'Max Moving Average Acceleration 70G=' Max_70_2_smooth};
% annotation('textbox',[.2 .75 .1 .1],'String',str,'FitBoxToText','on');

figure('Name','Run 2 - 500G')
plot(Run2_time,Run2_500,'-o','LineWidth',1,'color','k')
hold on
plot(Run2_time,Run2_500smooth,'-d','LineWidth',1,'color','r')
hold on

title('Acceleration v. Time for Full Scale Drop Test from 0.2032 m')
xlabel('Time [s]')
ylabel('Acceleration [G-forces]')
legend('500G Sensor Data','500G Moving Average')
str = {'Max Measured Acceleration 500G=' Max_500_2,...
    'Max Moving Average Acceleration 500G=' Max_500_2_smooth};
annotation('textbox',[.2 .75 .1 .1],'String',str,'FitBoxToText','on');


%%%%%%%%%%%%%%%%%%%%%%%%%%%%%%%%%%%%%%%%%%%%%%%%%%%%%%%%%%%%%%%%%%%%%%%
% Run 3 Results with 500G Sensor (70G Cable Severed During Run 3)
%%%%%%%%%%%%%%%%%%%%%%%%%%%%%%%%%%%%%%%%%%%%%%%%%%%%%%%%%%%%%%%%%%%%%%%

```

```
% Create matrices for time and 500G data
Run3 = csvread('Run3.csv',1,0);
Run3_time = Run3([1:end],[1]);
Run3_time = Run3_time - Run3_time(1,1);
Run3_500 = Run3([1:end],[3]);

% Determine window size for moving average by plotting the sum of absolute
% differences for different window sizes and finding the knee in the curve,
% where the window is smallest and the curve seems to flatten. Maximum
% window size is calculated from a 10 kHz sample rate over the duration of
% the impulse.
windowSizes = 1 : 1 : 26;
for k = 1 : length(windowSizes);
    smoothed500 = movmean(Run3_500, windowSizes(k));
    sad500(k) = sum(abs(smoothed500 - Run3_500));
end

figure('Name','Run 3 - SAD')
plot(windowSizes, sad500, 'b*-', 'LineWidth', 2);
title('SAD Run 3 500G')
grid on;
xlabel('Window Size');
ylabel('Sum of Absolute Differences');

% Moving Average Filter
Run3_500smooth = smoothdata(Run3_500,'movmean');

% Find maximum accelerations captured by each sensor
Max_500_3 = max(abs(max(Run3_500)),abs(min(Run3_500)));
Max_500_3_smooth = max(abs(max(Run3_500smooth)),abs(min(Run3_500smooth)));

```

```
% Plot raw and smooth data on single figure
figure('Name','Run 3 - 500G')
plot(Run3_time,Run3_500,'-+','LineWidth',1,'color','k')
hold on
plot(Run3_time,Run3_500smooth,'-d','LineWidth',1,'color','r')
hold on

title('Acceleration v. Time for Full Scale Drop Test from 1.524 m')
xlabel('Time [s]')
ylabel('Acceleration [G-forces]')
legend('500G Sensor Data','500G Moving Average')
str = {'Max Measured Acceleration 500G=' Max_500_3,...
    'Max Moving Average Acceleration 500G=' Max_500_3_smooth};
annotation('textbox',[.2 .75 .1 .1],'String',str,'FitBoxToText','on');


%%%%%%%%%%%%%%%%%%%%%%%%%%%%%%%%%%%%%%%%%%%%%%%%%%%%%%%%%%%%%%%%%%%%%%%
% Run 4 Results with 500G Sensor (70G Cable Severed During Run 3)
%%%%%%%%%%%%%%%%%%%%%%%%%%%%%%%%%%%%%%%%%%%%%%%%%%%%%%%%%%%%%%%%%%%%%%%

% Create matrices for time and 500G data
Run4 = csvread('Run4.csv',1,0);
Run4_time = Run4([1:end],[1]);
Run4_time = Run4_time - Run4_time(1,1);
Run4_500 = Run4([1:end],[2]);

% Determine window size for moving average by plotting the sum of absolute
% differences for different window sizes and finding the knee in the curve,
% where the window is smallest and the curve seems to flatten. Maximum
% window size is calculated from a 10 kHz sample rate over the duration of
% the impulse.
```

```
windowSizes = 1 : 1 : 26;
for k = 1 : length(windowSizes);
    smoothed500 = movmean(Run4_500, windowSizes(k));
    sad500(k) = sum(abs(smoothed500 - Run4_500));
end

figure('Name','Run 4 - SAD')
plot(windowSizes, sad500, 'b*-', 'LineWidth', 2);
title('SAD Run 4 500G')
grid on;
xlabel('Window Size');
ylabel('Sum of Absolute Differences');

% Moving Average Filter
Run4_500smooth = smoothdata(Run4_500,'movmean');

% Find maximum accelerations captured by each sensor
Max_500_4 = max(abs(max(Run4_500)),abs(min(Run4_500)));
Max_500_4_smooth = max(abs(max(Run4_500smooth)),abs(min(Run4_500smooth)));

% Plot raw and smooth data on single figure
figure('Name','Run 4 - 500G')
plot(Run4_time,Run4_500,'-+','LineWidth',1,'color','k')
hold on
plot(Run4_time,Run4_500smooth,'-d','LineWidth',1,'color','r')
hold on

title('Acceleration v. Time for Full Scale Drop Test from 0.8128 m')
xlabel('Time [s]')
ylabel('Acceleration [G-forces]')
legend('500G Sensor Data','500G Moving Average')
```

```
264 str = {'Max Measured Acceleration 500G=' Max_500_4,...
265     'Max Moving Average Acceleration 500G=' Max_500_4_smooth};
266 annotation('textbox',[.2 .75 .1 .1],'String',str,'FitBoxToText','on');
```

Appendix E

Drawings

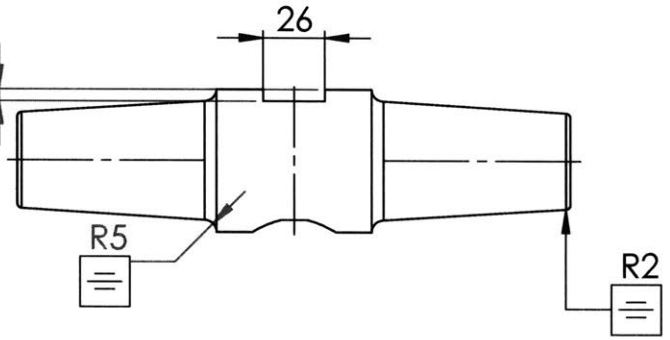

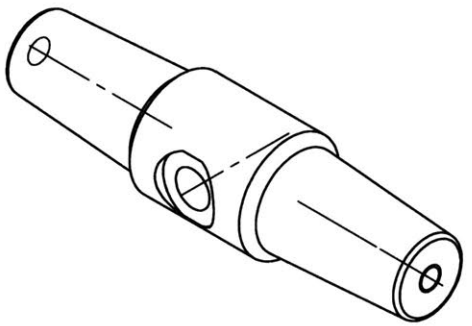

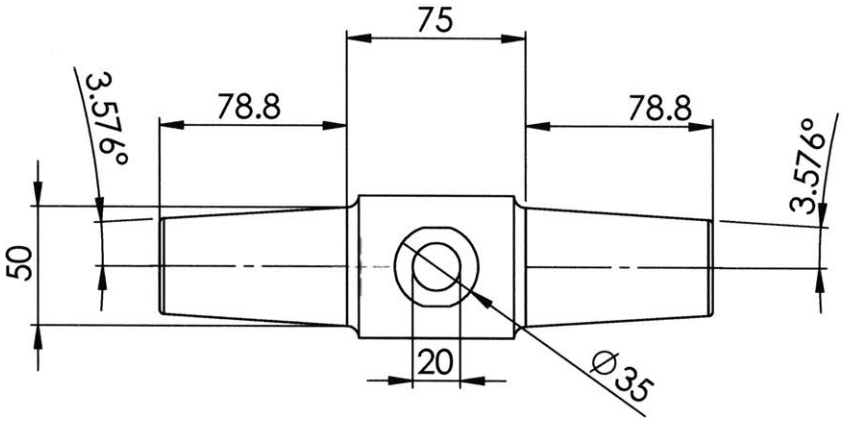

Ø 10.72 ↧ 50
1/2-13 UNC ↧ 30

Ø 10.72 ↧ 50
1/2-13 UNC ↧ 30

UNLESS OTHERWISE SPECIFIED: DIMENSIONS ARE IN MILLIMETERS SURFACE FINISH: 16 TOLERANCES: LINEAR: ANGULAR:		FINISH:				DEBURR AND BREAK SHARP EDGES	DO NOT SCALE DRAWING	REVISION
	NAME	SIGNATURE	DATE				TITLE: Shock Test Shaft	
DRAWN	Michael Beautyman		2017.03.21					
CHK'D								
APPV'D								
MFG								
Q.A				MATERIAL: 1018 Cold Rolled Steel			DWG NO. 1	A4
				WEIGHT:			SCALE:1:3	SHEET 1 OF 1

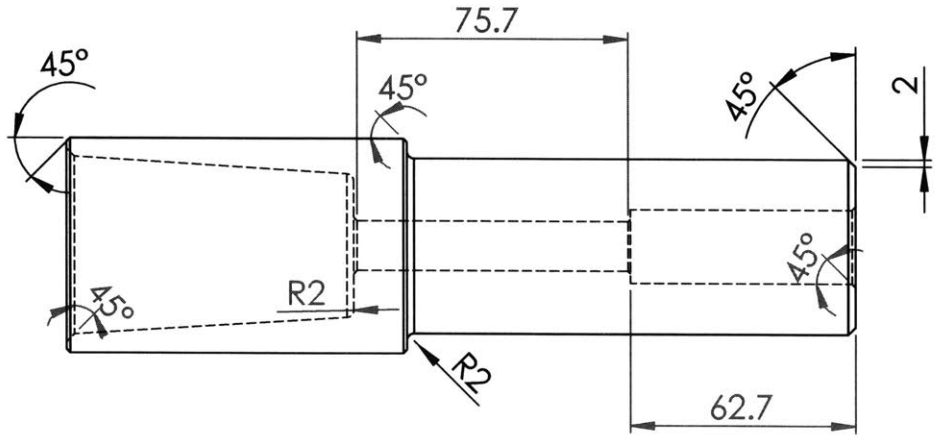

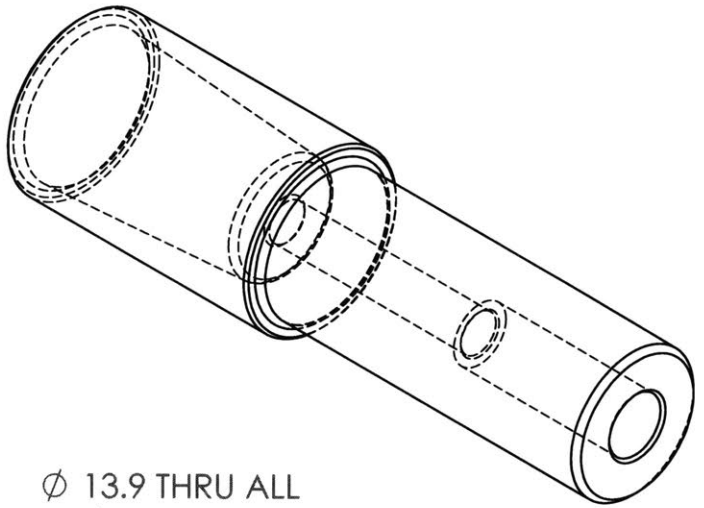

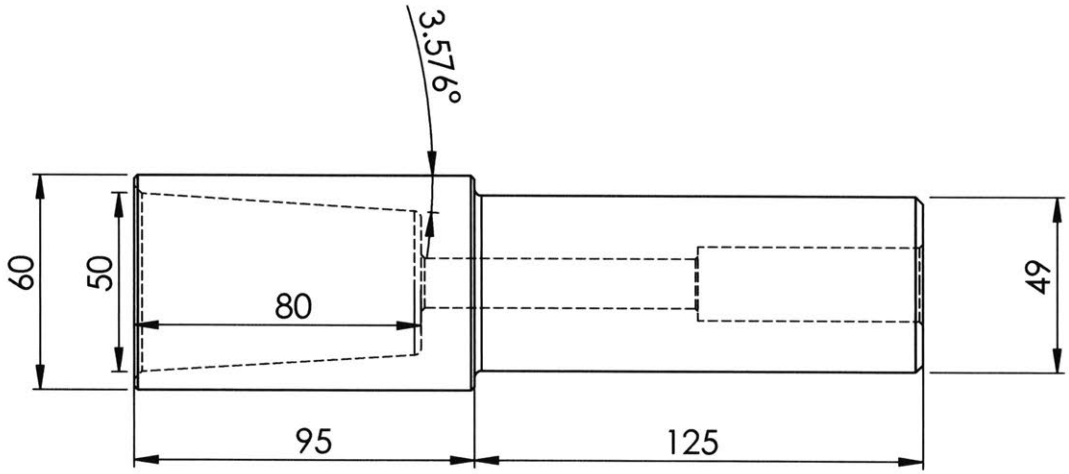

∅ 13.9 THRU ALL
⌴ ∅ 20.6 ↧ 62.70
⌵ ∅ 15.2 X 90°, Mid Side

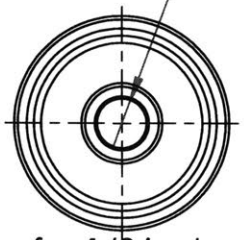

Counterbore for 1/2 inch socket head screw

UNLESS OTHERWISE SPECIFIED: DIMENSIONS ARE IN MILLIMETERS SURFACE FINISH: 16 TOLERANCES: LINEAR: ANGULAR:		FINISH:			DEBURR AND BREAK SHARP EDGES	DO NOT SCALE DRAWING	REVISION 1
	NAME	SIGNATURE	DATE			TITLE: Test Flange	
DRAWN	Michael Beautyman		2017.03.21				
CHK'D							
APPV'D							
MFG							
Q.A				MATERIAL: 1018 Cold Rolled Steel		DWG NO.	A4
				WEIGHT:		SCALE:1:2	SHEET 1 OF 1

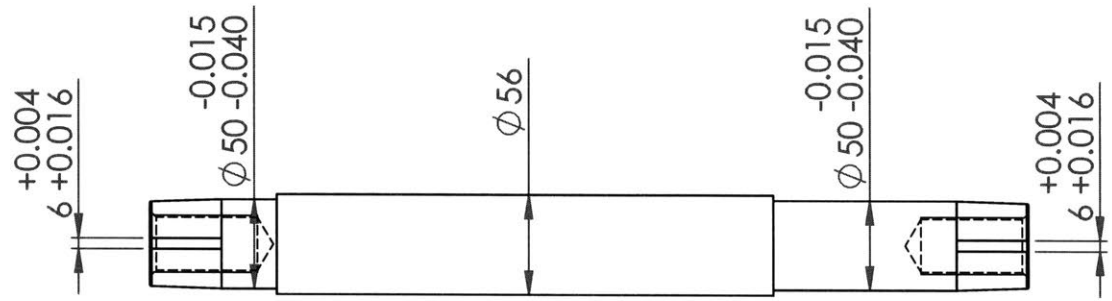

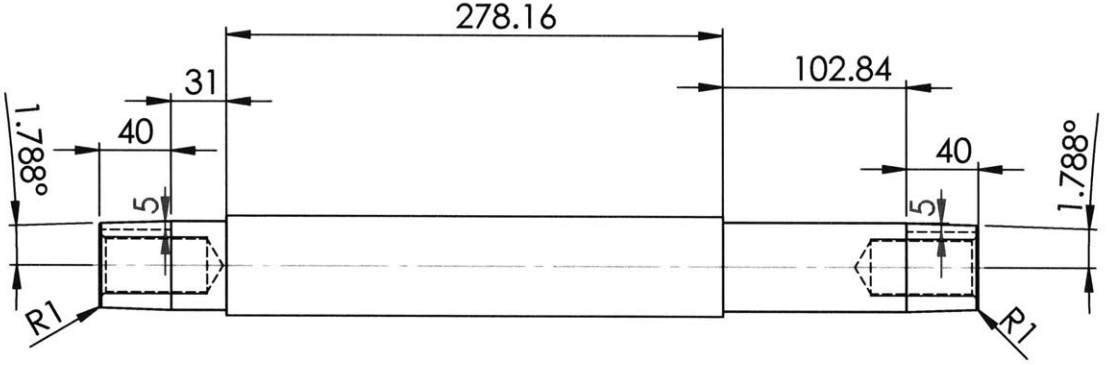

Ø 29.77 ↧ 60
1-1/4-12 UNF - 6H ↧ 60

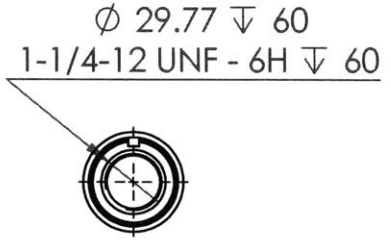

Ø 29.77 ↧ 60
1-1/4-12 UNF - 6H ↧ 60

UNLESS OTHERWISE SPECIFIED: DIMENSIONS ARE IN MILLIMETERS SURFACE FINISH: 16 TOLERANCES: LINEAR: ANGULAR:		FINISH: 16 ON TAPER		DEBURR AND BREAK SHARP EDGES		DO NOT SCALE DRAWING	REVISION
	NAME	SIGNATURE	DATE			TITLE:	
DRAWN						Beautyman Tilt Shaft	
CHK'D							
APPV'D							
MFG							
Q.A				MATERIAL: 1018 STEEL		DWG NO.	A4
				WEIGHT:		SCALE:1:4	SHEET 1 OF 1

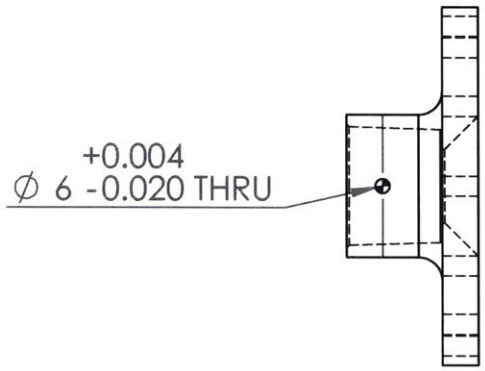

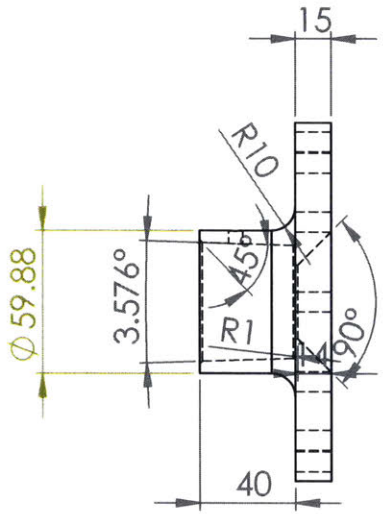

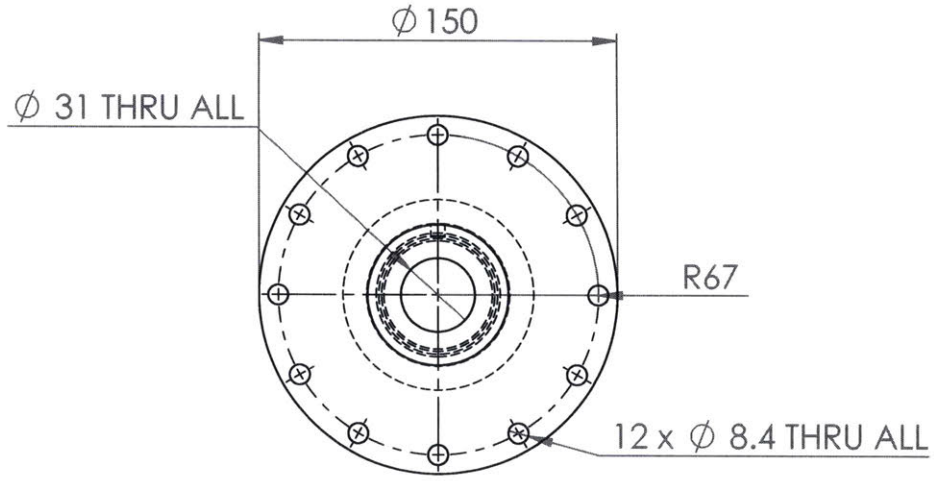

NOTE: Please manufacture 2 of this part

UNLESS OTHERWISE SPECIFIED: DIMENSIONS ARE IN MILLIMETERS SURFACE FINISH: 16 inside taper TOLERANCES: LINEAR: ANGULAR:	FINISH: 16 SURFACE FINISH INSIDE TAPER	DEBURR AND BREAK SHARP EDGES	DO NOT SCALE DRAWING / REVISION

	NAME	SIGNATURE	DATE
DRAWN			
CHK'D			
APPV'D			
MFG			
Q.A			

MATERIAL:
1018 STEEL

WEIGHT:

TITLE:
Beautyman Tilt Flange

DWG NO. A4

SCALE:1:3

SHEET 1 OF 1

18-8 Shoulder Screw 1/2 diameter x 3" long shoulder, 3/8-16 thread size

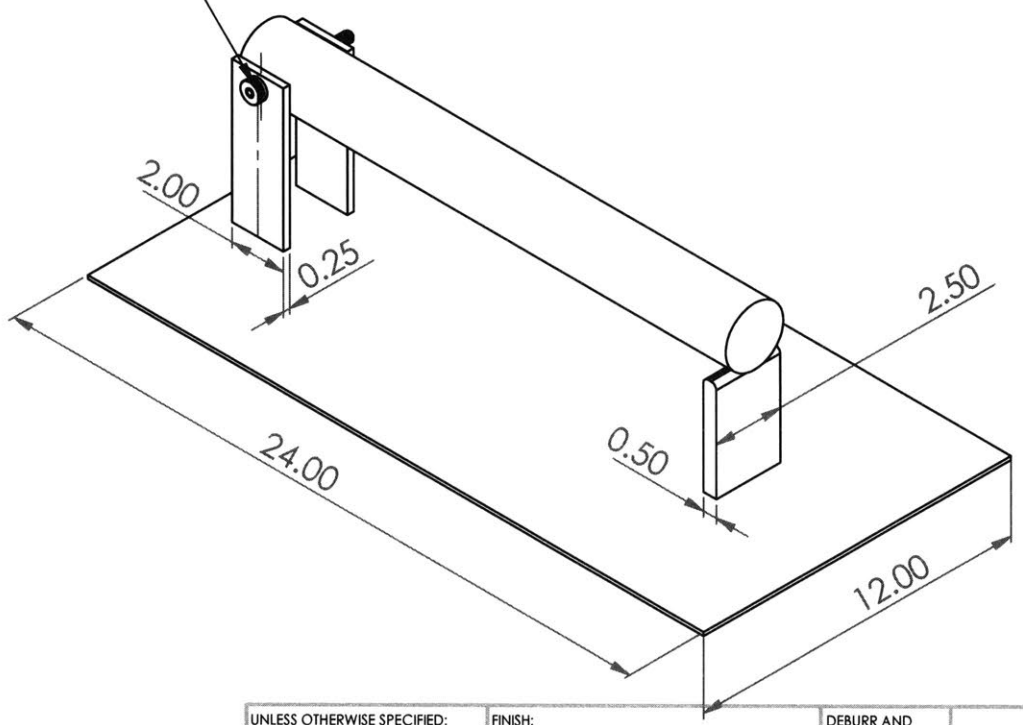

UNLESS OTHERWISE SPECIFIED: DIMENSIONS ARE IN INCHES SURFACE FINISH: TOLERANCES: LINEAR: ANGULAR:		FINISH:			DEBURR AND BREAK SHARP EDGES	DO NOT SCALE DRAWING	REVISION
	NAME	SIGNATURE	DATE			TITLE:	
DRAWN						Simply Supported Beam	
CHK'D							
APPV'D							
MFG							
Q.A				MATERIAL:		DWG NO.	A4
				WEIGHT:		SCALE:1:5	SHEET 1 OF 1

Bibliography

[DIN, 2001] (2001). Din 7190 interference fits (calculation and design rules). Standard, Deutsches Institut fur Normung.

[DIN, 2008] (2008). Din 69063-1 machine tools - tool receiver for hollow taper shanks. Standard, Deutsches Institut fur Normung.

[DIN, 2011] (2011). Din 69893-1 hollow taper shanks with flange contact surface - part 1: Hollow taper shanks type a and type c; dimensions and design. Standard, Deutsches Institut fur Normung.

[DNV, 2015] (2015). Rules for classification: Ships — DNVGL-RU-SHIP-Pt3Ch14 Rudders and Steering. Standard, DNV GL.

[Agapiou, 2005] Agapiou, J. S. (2005). A methodology to measure joint stiffness parameters for toolholder-spindle interfaces. *Journal of Manufacturing Systems*, 24:13–20.

[Akar, 2017] Akar (2017). Single stage multi leaf spring. `http://www.akartoolsltd.com/products/leaf-springs/multi-leaf-spring.html`. Accessed: 2017-05-08.

[AnimatedKnots, 2016] AnimatedKnots (2016). Tumble hitch tying. `http://www.animatedknots.com/tumble/#ScrollPoint`.

[Bashir Asdaque and Behera, 2014] Bashir Asdaque, P. M. G. and Behera, R. K. (2014). Vibration Analysis of Hollow Tapered Shaft Rotor. *Advances in Acoustics & Vibration*, pages 1–14.

[Bosch, 2004] Bosch (2004). *Bosch Automotive Handbook (sixth edition)*. Plochingen : Robert Bosch ; London : Distribution, Professional Engineering Publishing, 2004.

[Bossmanns and Tu, 2002] Bossmanns, B. and Tu, J. F. (2002). Conceptual Design of Machine Tool Interfaces for High-Speed Machining. *Journal of Manufacturing Processes*, 4:16–27.

[Creitaru and Grigore, 2011] Creitaru, A. and Grigore, N. (2011). Tribological considerations regarding the functional domain determination of the conical fit assembly. *Machine Design*, 3(3):199–204.

[Endevco, 2016] Endevco (2016). Acceleration Levels of Dropped Objects. White paper, Endevco Meffitt Sensing Systems.

[FESD, 2009] FESD (2009). Screw Thread Design. White paper, Fastenal Engineering & Design Support.

[Goyal and Buratynski, 2000] Goyal, S. and Buratynski, E. K. (2000). Methods for realistic drop-testing. *The International Journal of Microcircuits and Electronic Packaging*, 23(1):45–52.

[Hanna et al., 2002] Hanna, I., Agapiou, J., and Stephenson, D. (2002). Modeling the HSK toolholder-spindle interface. *JOURNAL OF MANUFACTURING SCIENCE AND ENGINEERING-TRANSACTIONS OF THE ASME*, 124(3):734–744.

[IDM, 2013] IDM (2013). Release hook specification sheets. `http://www.idminstruments.com.au/products/droptestreleasehooks`.

[Kang et al., 2015] Kang, J., Bae, J., On, H., and Kwon, Y. (2015). Tapered Joint Design for Power Transmission of MW-grade Wind Turbine. *Transactions of the Korean Society of Mechanical Engineers A*, 39(11):1183–1189.

[Kausel, 2016] Kausel, E. (2016). Interview regarding shock testing and impulses. personal communication.

[Kocherovsky, 2000] Kocherovsky, E. (2000). An HSK primer. *Manufacturing Engineering*, 124(5):66–80.

[Lewis, 1999] Lewis, D. L. (1999). What's happening with HSK? *Manufacturing Engineering*, 122(1):78–82.

[Ling Xiong et al., 2013] Ling Xiong, Peng Shang, and Youlin Xu (2013). Exact Solution of Stress and Radial Displacement of Elastic Tapered Interference Fit. *Applied Mechanics and Materials*, 423-426(423-426):1438–1443.

[LR, 1982] LR (1982). Rules for classification: Ships — Ch13 Ship Control Systems. Standard, Lloyd's Register.

[McMaster-Carr, 2017] McMaster-Carr (2017). Product catalog. `https://www.mcmaster.com/#`.

[Mermoz, 2007] Mermoz, E. (2007). Coupling flange system for hollow shaft.

[Mills, 2016] Mills, N. (2016). Design and Testing of a Pan-tilt Mechanism for Severe Environments. Master's thesis, Massachusetts Institute of Technology, Mechanical Engineering Department.

[NIST, 2017] NIST (2017). Charpy impact testing. https://www.nist.gov/image-18710. Accessed: 2017-05-08.

[Peterson and Wahl,] Peterson, R. and Wahl, A. Fatigue of shafts at fitted members, with related photo-elastic analysis. *Journal of Applied Mechanics*, 57:A1–A11.

[Schauer, 1962] Schauer, H., editor (1962). *Shock Resistance Testing of U.S. Naval Vessels*. SNAME.

[Shepstone, 2005] Shepstone, S. (2005). Propeller Installation Calculations for US Navy Ships. Unpublished Manuscript.

[Slocum, 2008] Slocum, A. H. (2008). Fundamentals of design. http://pergatory.mit.edu/resources/FUNdaMENTALS.html.

[Slocum, 2011] Slocum, A. H. (2011). Hertz point contact design spreadsheet.

[Slocum, 2014] Slocum, A. H. (2014). Proposal for A Low-Torque Pan Tilt System for Directional Scanning in a Marine Environment. Unpublished Work.

[Vable, 2002] Vable, M. (2002). *Mechanics of materials*. New York : Oxford University Press, 2002.